Selection on ancient variations drives the adaptive radiation of *Metrosideros* across the Hawaiian archipelago

Jae Young Choi[a,*], Xiaoguang Dai[b], Julie Z. Peng[c], Priyesh Rughani[b], Scott Hickey[d], Eoghan Harrington[b], Sissel Juul[b], Julien Ayroles[c], Michael Purugganan[a], and Elizabeth A. Stacy[e,*]

[a]Center for Genomics and Systems Biology, Department of Biology, New York University, New York, New York, USA

[b]Oxford Nanopore Technologies Inc., New York, New York, USA

[c]Department of Ecology and Evolutionary Biology, Princeton University, Princeton, New Jersey, USA

[d]Oxford Nanopore Technologies Inc., San Francisco, California, USA

[e]School of Life Sciences, University of Nevada Las Vegas, Las Vegas, Nevada, USA

*Corresponding authors: JYC (jyc387@nyu.edu) and EAS (elizabeth.stacy@unlv.edu)

Abstract

Adaptive radiations display a remarkable suite of phenotypic and ecological variation and recent genome sequencing studies have shed light on the evolutionary processes and genomic architectures underlying this variation. Our understanding of the genomic architecture of adaptive radiations is largely incomplete, however, as studies have been biased towards animal and continental systems. We conducted a genomic analysis of *Metrosideros*, a landscape-dominant and incipient adaptive radiation of woody plants that spans a striking range of phenotypes and environments across the Hawaiian archipelago. Using the nanopore-sequencing platform, we created the first chromosome-level genome assembly for this group and analyzed whole-genome sequences of 131 individuals from 11 taxa sampled across the islands. Population structure analysis revealed that taxa grouped by island and supporting previous studies, but gene flow occurred extensively within and between island lineages. Demography modeling showed concordance between the divergence times of island-specific lineages and the geological formation of individual islands. The genome-wide differentiation landscape was investigated to characterize patterns of selection and revealed that differentiation outliers harbored divergent haplotypes that potentially predate the Hawaiian radiation. These same regions showed evidence of selective sweeps across the archipelago, indicating an archipelago-wide shared selective pressure for divergent haplotypes. Further, genomic regions with lineage-specific evidence of selection also harbored ancient haplotypes. We conclude that the genomic architecture of adaptive radiation in Hawaiian *Metrosideros* arises from selection on ancient divergent haplotypes that formed early, before the initial colonization of the archipelago and were recurrently selected as lineages colonized and diversified on new islands.

Introduction

Adaptive radiations exhibit extraordinary levels of morphological and ecological diversity (Gillespie et al. 2020). Although definitions of adaptive radiation vary among authors (Schluter 2000; Futuyma 1998; Losos 2010; Givnish 2015; Simpson 1944; Glor 2010), all center on ecological opportunity as a driver of adaptation and, ultimately, diversification (Givnish 1997; Losos 2009; Schluter 2000; Simpson 1953). Divergent selection, the primary mechanism underlying adaptive radiations, favors phenotypes of opposite extremes (Rundle and Nosil 2005) and selects alleles in each population that confer adaptation to an unoccupied or under-utilized ecological niche. Differential adaptation results in divergence and, ultimately, reproductive isolation between populations (Schluter 2009). Adaptive radiations demonstrate the remarkable power of natural selection as a driver of biological diversity, and they provide excellent systems for studying the evolutionary processes involved in diversification and speciation (Wilson 1992).

Remote oceanic islands are attractive systems for the study of adaptive radiations. Within a volcanic island chain, the formation of each new island presents a blank slate for colonization and diversification such that each island can be thought of as a replicate natural evolutionary "experiment" (Losos and Ricklefs 2009). Colonization of remote islands often involves population bottlenecks (Frankham 1997), making adaptive radiations in such settings especially impressive and even paradoxical, given the generation of high species richness from an initially limited gene pool (Martin and Richards 2019). Several classic examples of adaptive radiation derive from archipelagos, such as Darwin's finches from the Galapagos islands (Grant and Grant 2008), anole lizards from the Caribbean islands (Losos 2009), Hawaiian Drosophilids (Carson and Kaneshiro 1976), and Hawaiian silverswords (Robichaux et al. 1990) to name a few. These examples have been crucial to our understanding of the biological factors involved in adaptive radiations, especially demonstrating the primary role of ecology in diversification (Schluter 2000). Ecology, however, is just one component of the process. Genes and genomes define the phenotypic space from which diversifying selection can forge adaptation to contrasting environments. Without insights into the underlying genetic basis of diversification, our understanding of adaptive radiations will remain

incomplete. Such insights have been hindered by the difficulty of genetic manipulations and controlled-environment experiments with non-model organisms, which make up the majority of lineages undergoing adaptive radiation.

Major breakthroughs in the genetics of adaptive radiation were made with the arrival of genome sequencing technology. By examining sequences of multiple individuals from their natural environment, it became possible to "catch in the act" the speciation processes that have occurred between incipient lineages (Wolf and Ellegren 2017). But population genomic studies of island adaptive radiations have been biased towards animal systems, in particular, birds and fishes (Berner and Salzburger 2015; Seehausen et al. 2014; Marques et al. 2019) with no equivalent studies in plants. The eco-evolutionary scenarios associated with adaptive radiations are diverse, however, (Olson and Arroyo-Santos 2009; Givnish 2015), and whether commonalities identified in adaptive radiations in animals (Berner and Salzburger 2015; Campbell et al. 2018) are applicable to plants is an open question. For instance, population genomic studies of animal lineages reveal that diversification is typically facilitated by allopatry, but diversification in plants often involves geographically overlapping populations responding to variation in the local environment (Anacker and Strauss 2014). This observation highlights the importance of divergent selection in the early stages of speciation in plants and suggests that plant clades undergoing adaptive radiation will be excellent model systems for studying the genomics of ecological diversification. In particular, incipient adaptive radiations of plants on islands will allow insights into the genomic architecture of early-stage radiation.

We investigated the evolutionary genomics of adaptive radiation in *Metrosideros* Banks ex Gaertn. (Myrtaceae) across the Hawaiian archipelago. Hawaiian *Metrosideros* is a landscape-dominant, hypervariable and highly dispersible group of long-lived [> 650 years] (Hart 2010) woody taxa that are non-randomly distributed across Hawaii's famously heterogeneous landscape, including cooled lava flows, wet forests and bogs, subalpine zones, and riparian zones (Stacy and Sakishima 2019; Dawson and Stemmermann 1990). About 25 taxa are distinguished by their vegetative characters ranging from prostate plants that flower a few centimeters above ground to 30-m tall trees, and leaves range dramatically in size, shape, pubescence, color, and rugosity (Sur et

al. 2018; Stacy and Sakishima 2019; Stacy et al. 2020). Variation in leaf mass per area within the four *Metrosideros* taxa on Hawaii Island alone matches that observed for woody species globally (Tsujii et al. 2016). Common garden experiments (Cordell et al. 1998, 2000; Corn and Hiesey 1973; Kitayama et al. 1997; Stemmermann 1983; Stacy et al. 2020) and parent-offspring analysis (Stacy et al. 2016) demonstrate heritability of taxon-diagnostic vegetative traits, indicating that taxa are distinct genetic groups and not the result of phenotypic plasticity. Taxa display evidence of local adaptation to contrasting environments (Ekar et al. 2019; Morrison and Stacy 2014), suggesting that ecological divergent selection is responsible for diversification within the group (Stacy et al. 2014). This diversification has occurred within the past ~3.1-3.9 million years (MY) (Percy et al. 2008; Dupuis et al. 2019) in spite of the group's exceptional dispersibility by way of showy bird-pollinated flowers and tiny wind-dispersed seeds (Dawson and Stemmermann 1990). Lastly, the presence of partial reproductive isolating barriers between taxa is consistent with the early stages of speciation (Stacy et al. 2017). Here, we generated several genomic resources to gain a deeper insight into the evolutionary processes underlying the incipient adaptive radiation of *Metrosideros* in Hawaii.

Results

Generating a genomic resource for Hawaiian *Metrosideros*. Using the nanopore sequencing platform, an individual *Metrosideros polymorpha* var. *incana* was whole-genome sequenced at 66× coverage (see Supplemental Table 1 for genome sequencing statistics). The reads were assembled into a draft assembly that had high contiguity with a contig N50 of 1.85 Mbp (Table 1). We then implemented Pore-C sequencing (Ulahannan et al. 2019), which combines chromosome conformation capture with long-read nanopore sequencing, to assay the *Metrosideros*-specific chromosome contact map and anchor the contigs into their correct chromosomal positions [see Supplemental Table 2 for Pore-C sequencing statistics] (Kaplan and Dekker 2013). Using the Pore-C contact maps, the initial assembly contigs were scaffolded into 11 super-scaffolds (Fig. 1A) spanning 292.8 Mbps with a N50 of 25.9 Mbp. Importantly, the number of super-scaffolds was consistent with the 11 chromosomes in *Metrosideros* (Carr 1978). The assembly was evaluated with 2,326 Benchmarking Universal Single-Copy Ortholog (BUSCO) genes from eudicots,

and 2,183 genes (93.8%) were present. These results, in the end, suggested that our chromosome-level genome assembly was highly contiguous and complete. Gene annotation was conducted using the nanopore sequencing of a cDNA library generated from leaf tissue (see Supplemental Table 3 for cDNA sequencing statistics). A total of 28,270 genes were predicted with 94.2% of the transcripts showed an annotation edit distance (AED) of less than 0.5.

Table 1. Genome assembly statistics for *M. polymorpha* var. *incana*.

Assembly features	
# of contigs	1,035
# of scaffolded psuedomolecules	11
Total number of bases in contigs	307,350,354 bp
Total number of bases scaffolded	292,766,828 bp
Maximum contig length	8,272,703 bp
Contig N50 length	1.852 Mbp
Scaffold N50 length	25.93 Mbp
BUSCO score	93.8%
GC content	39.8%
Repeat content	36.3%
Number of annotated genes	28,270

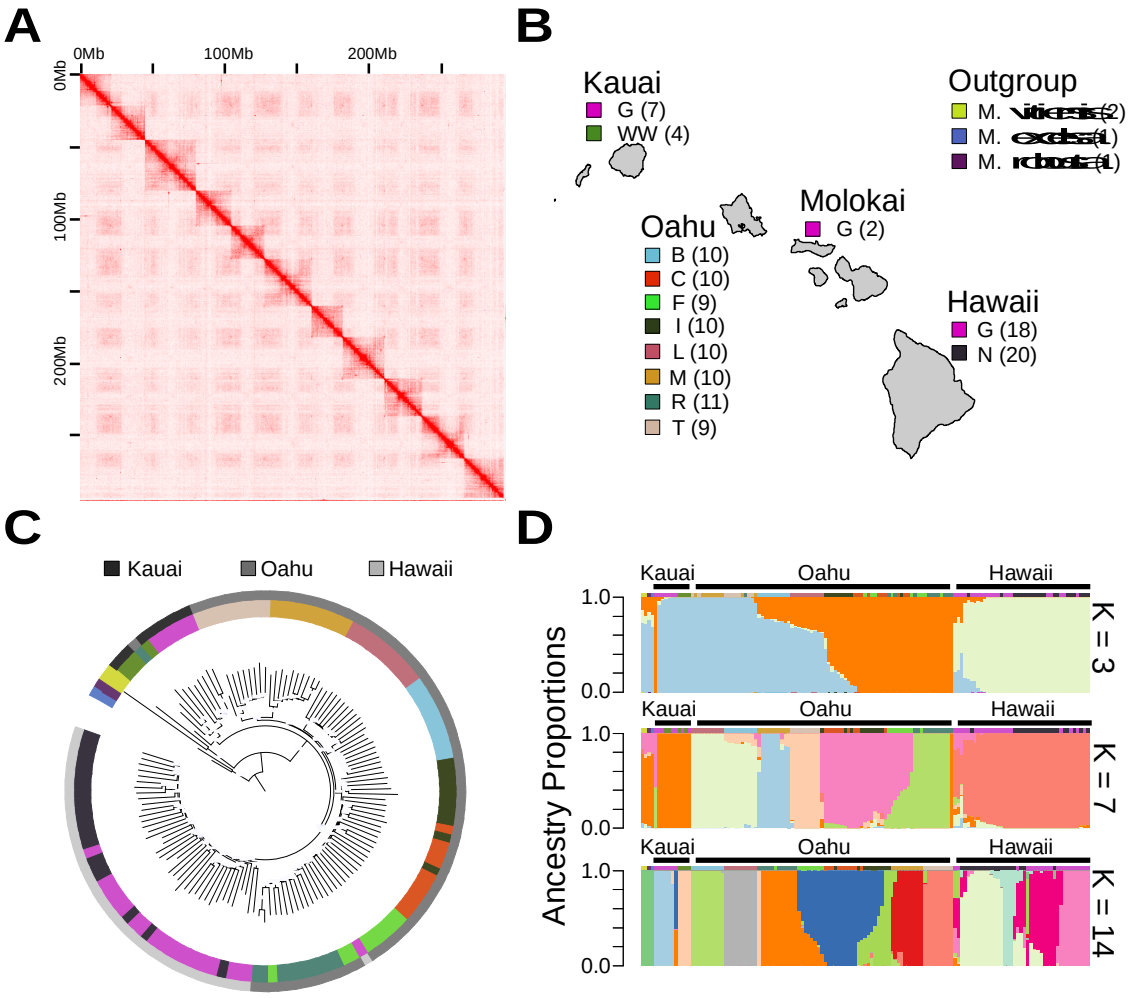

Figure 1. Genomics of Hawaiian *Metrosideros*. (A) Pore-C-based chromosome contact matrix for *M. polymorpha* var. *incana*. (B) Geographic distribution and taxon classification for the 135 samples that were analyzed in this study. Taxa are abbreviated as *M. polymorpha* race B [B], *M. polymorpha* race C [C], *M. polymorpha* race F [F], *M. polymorpha* race L [L], *M. polymorpha* var. *glaberrima* [G], *M. polymorpha* var. *incana* [I], *M. macropus* [M], *M. polymorpha* var. *newellii* [N], *M. polymorpha* var. *waialealae* [WW], *M. rugosa* [R], and *M. tremuloides* [T]. Numbers in parentheses represent sample sizes. (C) Genome-wide neighbor-joining tree built using a distance matrix. Outer circle colors indicate island of origin for each sample, and inner circle colors indicate taxa as in panel (B). Nodes with greater than 95% bootstrap support are indicated with light blue circles. (D) Ancestry proportion estimates using the ADMIXTURE algorithm for K = 3, 7, and 14. Colors above admixture barplots represent taxa as in panel (B).

The population genomics of Hawaiian *Metrosideros* was investigated by whole-genome sequencing 89 individuals from the islands of Oahu and Kauai, and combining these sequencing data with previously published sequences from Hawaii Island and Molokai (Choi et al. 2020). In addition, we sequenced 4 *Metrosideros* species outside of the Hawaiian archipelago as outgroup genomes. In sum, we analyzed 131 individuals belonging to 11 taxa across the Hawaiian archipelago (Figure 1B). The median genome coverage was 14× per individual, and on average 93% of the sequencing reads were aligned to our reference genome (Supplemental Table 4). The mapped population genomic data were used to call SNPs, and after filtering there were 22,511,205 variable sites that were used for subsequent analysis.

Population structure and relationships across the Hawaiian archipelago. A neighbor-joining phylogenomic tree was reconstructed to examine the evolutionary relationships among populations (Fig. 2C). The tree topology showed a grouping of individuals by island with little evidence of recent migration between islands. Within the phylogeny, individuals clustered according to taxonomic designations and were monophyletic with high confidence (>95% bootstrap support). Exceptions were the paraphyletic relationships occurring among taxa C, F, and I on Oahu and taxa G and N on Hawaii Island. Among the outgroup species, *M. vitiensis* from the Pacific islands (Fiji and American Samoa) was sister to all Hawaiian *Metrosideros*.

Finer scale evolutionary relationships across Hawaiian *Metrosideros* were examined by estimating the ancestry proportions (K) for each individual (see Supplemental Figure 1 for K = 3 to K = 15 results). At K=3 most individuals from Kauai and Hawaii Island showed a single, island-specific ancestry component (Figure 2D). On Oahu, there were taxa with Oahu-specific ancestry (taxa C, F, and R), Kauai-specific ancestry (taxa M and T), and mixed Oahu and Kauai ancestry (taxa B, L, and I). With increasing K each taxon/population showed increasingly unique ancestry, and at K = 14, with few exceptions, individuals belonging to the same taxon/population shared a single, unique ancestry. One exception was taxon F, for which all individuals consistently showed admixed ancestry comprising components of both taxa C and R. Additionally, for

G and N on Hawaii Island, increasing K led to further subdivision of ancestry, consistent with the complex population substructure of Hawaii Island *Metrosideros* (Choi et al. 2020). On Hawaii Island, G belonged to two genetic groups designated G_{H1} and G_{H2} in our previous analysis, and G_{H2} represented a recently admixed population with taxon N (Choi et al. 2020). Taxon F on Oahu and population G_{H2} on Hawaii Island are likely to be hybrid populations formed from recent hybridization of genetically distinct populations (Mallet 2007). As such, they were removed from downstream analysis. We focused on 10 taxa/populations (B, C, G_{H1}, G from Kauai [G_K], I, L, M, N, R, and T), each of which had a largely single ancestry and sufficient sample sizes (minimum of 7 individuals in G_K and maximum of 14 individuals in taxa N) for population genomic analysis.

We investigated the evidence for gene flow between taxa by calculating Patterson's D-statistics (ABBA-BABA D test) (Green et al. 2010; Durand et al. 2011) on all population trios following the species-wide topology (Fig. 2C). *M. vitiensis* was used as the outgroup, specifically the sample from Fiji due to its high genome coverage. Overall, 85 of the 159 (53.5%) trio topologies had significant D-statistics (Bonferroni corrected p-value < 0.05; see Supplemental Figure 2 for results of each trio). Of the 85 trios, 53 (62.4%) topologies involved admixture between taxa on different islands, indicating that reticulate evolution was pervasive within and between islands. Taxa M and T, however, were an exception as they had the fewest significant D-statistics and no evidence of admixture with lineages outside of Oahu (Supplemental Figure 2).

Divergence times of *Metrosideros* across the islands. We investigated the speciation history of Hawaiian *Metrosideros* through demographic modeling. The population divergence times were estimated using the generalized phylogenetic coalescent sampler (G-PhoCS) (Gronau et al. 2011). From each island, a single population/taxon was chosen as a representative since we were interested in the colonization history of *Metrosideros* across the islands. Populations of the archipelago-wide taxon G were chosen from each island, except Oahu, for which G samples were not available. Thus, taxon M was chosen to represent Oahu, as it had no significant evidence of between-island admixture (Supplemental Figure 2), which reduced the number of admixture models to be tested with G-PhoCS.

Initially, we ran G-PhoCS models fitting migration bands (*i.e.* admixture) between terminal lineages. Results showed that parameterizing admixture had no effect on the estimates of divergence times (Supplemental Figure 3). Given this result, we based our divergence time analysis on the simple no-migration model. G-PhoCS estimated the divergence time between Hawaiian *Metrosideros* and the outgroup *M. vitiensis* at 4.36 million years ago [MYA] (95% Highest Posterior Density [HPD] 4.16 – 4.55 MYA), which is younger than the geological formation of Kauai (Fig. 2A). However, given that *M. vitiensis* is not the most closely related outgroup species to Hawaiian *Metrosideros* (Dupuis et al. 2019), the colonization of the Hawaiian Islands likely occurred more recently than 4.36 million years ago. Additionally, the divergence time estimates within Hawaii suggested that colonization of each island occurred long after its formation. The exception was Hawaii Island for which the divergence time of *Metrosideros* pre-dated the geological formation of that island. This result was also obtained in our previous study and discussed therein (Choi et al. 2020)

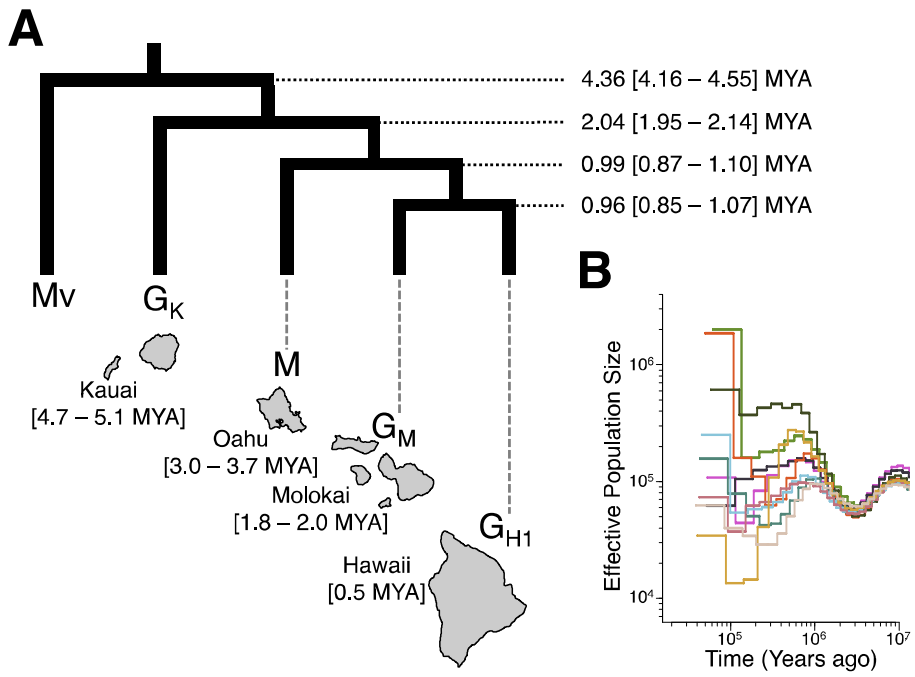

Figure 2. Divergence time and demographic history of Hawaiian *Metrosideros*. Relative times were converted to absolute times assuming a mutation rate of 7^{e-9} mutations per base pair per generation and a 20-year generation time. (A) G-PhoCS-estimated

divergence times for representative taxa from each island (above), and time of geological formation of each island based on Clague (Clague 1996) (below). (B) MSMC2 estimated effective population size for each Hawaiian taxon, color-coded as in Fig. 1B.

We used the program Multiple Sequentially Markovian Coalescent 2 [MSMC2] (Schiffels and Durbin 2014; Schiffels and Wang 2020) to estimate the past changes in effective population size (N_e) for each taxon/population. Results showed that all taxa had identical trajectories in ancient times showing a decrease in N_e until 3 MYA, followed by an increase and subsequent drop in N_e in a pattern unique to each taxon (Fig. 2B). This result suggests that all Hawaiian *Metrosideros* taxa share the same common ancestor that experienced a population bottleneck about 3 MYA when the ancestral population initially colonized the archipelago. Based on G-PhoCS and MSMC2 analysis the initial colonization of the Hawaiian archipelago was estimated to have occurred 3 – 4.4 MYA (150,000–220,000 generations ago).

The genomic landscape of differentiation. To investigate the genetic architecture underlying the *Metrosideros* radiation we narrowed our analysis to pairs of taxa that were phylogenetic sisters, since for these sisters their patterns of genome-wide differentiation would be a product of the early stages of speciation/radiation. For these sisters we used δaδi (Gutenkunst et al. 2009) to fit 20 different demography models (see Supplemental Table 5 for complete δaδi results) to find the best-fitting model. Results showed that pair G_{H1} and N and pair C and I were consistent with a speciation model in which lineage divergence occurred with continuous gene flow [*i.e.* primary gene flow] (Richards et al. 2019), while in pair B and L and pair M and T the populations have been largely isolated from each other with the exception of a recent or ancient gene flow event (Fig 3A).

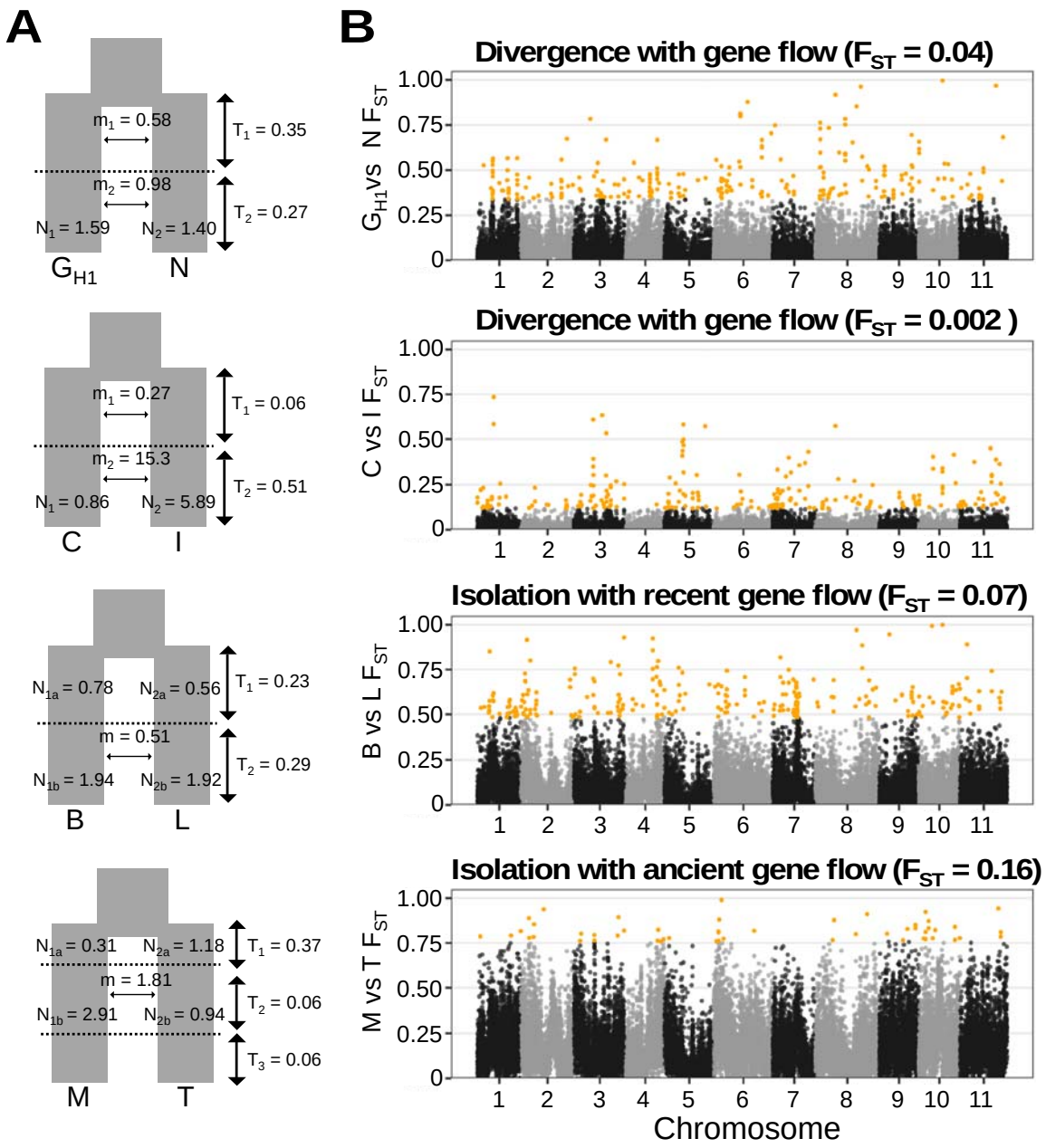

Figure 3. Genomic landscape of differentiation for the four phylogenetic sister pairs. (A) best-fitting demography model based on δaδi modeling. (B) Genome-wide F_{ST} in 10-kbp windows. Yellow dots are outliers identified with z-score-transformed F_{ST} values (zF_{ST}) > 4.

We investigated the genomic architecture of the adaptive radiation by quantifying the genome-wide patterns of differentiation and signatures of divergent selection occurring between sister taxa. We focused on differentiation (F_{ST}) outlier regions since

these regions would harbor the variations associated with the ecological divergence of the sister pairs (Via 2009). Results showed that in all four sister pairs differentiation outliers were scattered across all 11 chromosomes (Fig. 3B). Pair M and T had the fewest outlier windows (52 zF_{ST} outlier windows), while taxon pairs G_{H1} and N, C and I, and B and L had over 200 zF_{ST} outlier windows each (257, 226, and 260, respectively). The median genome-wide F_{ST} between M and T (F_{ST} = 0.16) was more than twice the level of F_{ST} within the other sister pairs (G_{H1} and N median F_{ST} = 0.04; C and I median F_{ST} = 0.002; B and L median F_{ST} = 0.07), suggesting that the increased genome-wide differentiation between M and T due to their genetic isolation may have eroded the outlier windows to undetectable levels (Renaut et al. 2013; Han et al. 2017). The genomic positions of the outlier windows generally did not overlap across the four sister-taxon pairs (*i.e.* >84% of the outlier windows were found in only one taxon pair; see Supplemental Figure 4).

Selection on ancient variation shapes the differentiation landscape. Genomic outliers of differentiation, however, do not always result from divergent selection (Cruickshank and Hahn 2014; Nachman and Payseur 2012; Noor and Bennett 2009), and F_{ST} can be a biased estimate of differentiation (Charlesworth 1998). Hence, as a complementary analysis we examined the levels of absolute genetic divergence (D_{xy}) within differentiation outlier regions, as D_{xy} is expected to be elevated in regions under divergent selection or regions acting as genetic barriers between populations (Cruickshank and Hahn 2014). Within each pair of sister taxa, D_{xy} levels were significantly elevated in differentiation outliers (MWU test p-value < 0.001) relative to the genomic background (Fig. 4A left box). Further, the differentiation outlier regions had significantly elevated D_{xy} levels when compared with other non-sister taxa representing increasing phylogenetic distances [MWU test p-value < 0.05] (Fig. 4A right box). Interestingly, the differentiation outliers had elevated D_{xy} even in comparisons with G_K on the oldest island, Kauai.

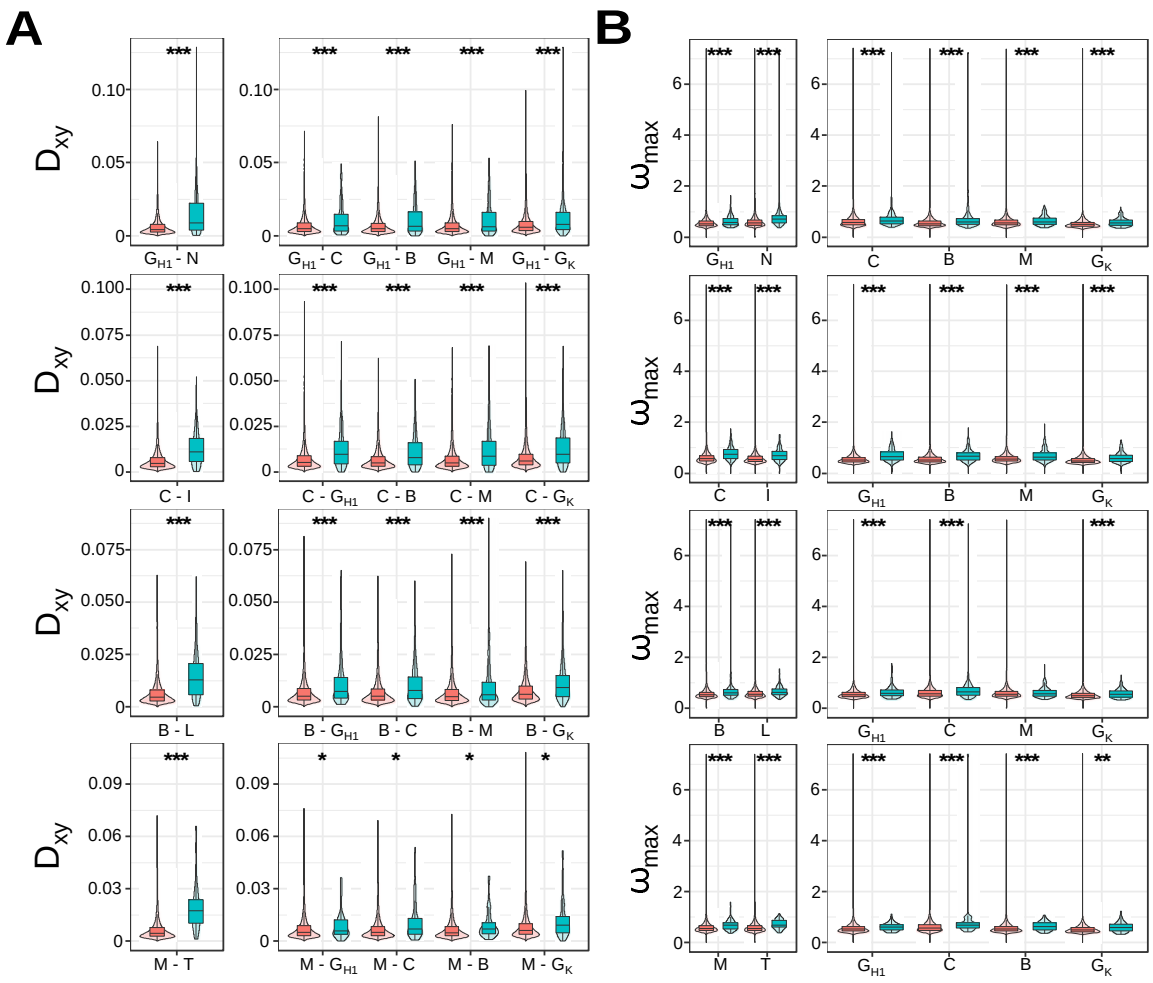

Figure 4. Sequence divergence and evidence of selective sweeps in differentiation outlier regions. Red boxes are statistics from the genomic background and green boxes are statistics from the differentiation outlier regions. (A) Sequence divergence (D_{xy}) statistics identified in a sister pair (left window) and D_{xy} estimated from the same regions but between one member of the pair and four other taxa representing increasing phylogenetic distances (right window). (B) Selective sweep statistics (ω_{max}) identified in a sister pair (left window) and the same regions in other *Metrosideros* taxa (right window). * indicate $p < 0.05$, ** indicate $p < 0.01$, and *** indicate $p < 0.001$.

We examined evidence of selective sweeps in differentiation outliers using ω_{max} statistics. Results showed that ω_{max} statistics were significantly higher for differentiation outlier regions (MWU test p-value < 0.001) than for the genomic background (Fig. 4B left box). Further, the same regions had significantly elevated ω_{max} statistics (MWU test

p-value < 0.01) in other taxa as well (Fig. 4B right box), indicating that differentiation outlier regions formed between sister pairs were also targets of positive selection in multiple other *Metrosideros* taxa.

The genomic analysis suggested that an archipelago-wide selective pressure had acted recurrently on the same genomic region across multiple *Metrosideros* taxa. Such recurrent selection can have profound effects on the genomic landscape of differentiation between populations (Burri et al. 2015; Stankowski et al. 2019). In *Metrosideros* we found that π, D_{xy}, F_{ST}, and ω_{max} were all positively and significantly correlated among taxa (Supplemental Figure 5). Because archipelago-wide selection is unlikely to be involved in the early-stage divergence of lineages, we examined regions that had evidence of lineage-specific accentuated differentiation. Using the correlated differentiation landscape as genomic controls (Burri 2017), we focused on regions that were significantly differentiated in a single sister pair (see Supplemental Table 6 for genomic positions). D_{xy} within the lineage-specific accentuated differentiation regions were significantly elevated compared to the genomic background (MWU test p-value < 0.001) [Supplemental Figure 6]. When compared to other non-sister taxa with increasing phylogenetic distances, the lineage-specific accentuated differentiation regions still had elevated D_{xy} levels compared to the genomic background (MWU test p-value < 0.01), except for the pair M and T.

A gene ontology (GO) enrichment analysis was conducted to determine the over-represented functional categories associated with the outlier windows. Results showed that genes within the outlier windows were enriched for 19 GO terms in the 'biological process' category, and the functions were largely related to metabolic processes, cell cycle, and immunity responses (Supplemental Figure 7).

Discussion

A major aim of this study was to understand the genomic architecture of an adaptive radiation within a remote archipelago. In plants, the molecular evolution of island adaptive radiations has been studied largely through a phylogenetic context by comparing the DNA sequence or genome of a single representative from each species within the radiating group (Nevado et al. 2019; Barrier et al. 1999). In contrast, we

investigated the population genomics of *Metrosideros* by constructing a chromosome-level genome assembly and sampling the genome-wide variation of 131 individuals across the Hawaiian archipelago. Using these novel genome resources we inferred the evolutionary history of Hawaiian *Metrosideros*, including the population divergence times and demography associated with the adaptive radiation. We discovered that selection on ancient variations played a major role in shaping the genome-wide differentiation landscape during the recent and historical radiation of this group across the Hawaiian archipelago.

Divergence time analysis yielded an estimate for the initial split between the common ancestor of all Hawaiian *Metrosideros* and the outgroup *M. vitiensis* at 4.4 MYA, when only Kauai, the oldest main island, was available for colonization (Clague 1996; Price and Clague 2002). Phylogeography and population structure analysis indicated that the radiation was endogenous to the islands wherein colonization and subsequent lineage diversification occurred within newly formed islands in the order of their appearance in the volcanic chain. This progressive colonization from older to younger islands [*i.e.* progression rule] (Wagner and Funk 1995) is a hallmark phylogeographic pattern for many Hawaiian flora and fauna (Shaw and Gillespie 2016). Our lower bound estimate of the initial colonization of Hawaii, however, was 3 MYA, when both Oahu and Kauai were available for colonization. In fact, morphotype diversity in *Metrosideros* is greatest on islands of intermediate age, especially Oahu (Stacy and Sakishima 2019), a pattern that might be expected if *Metrosideros* colonized the islands more recently when Oahu was largely vacant and Kauai was already colonized by lineages from the northwest Hawaiian Islands (*e.g.*, lobelioids (Givnish et al. 2009)). Unfortunately, with the available data, it is not possible to determine the order or exact timing of island colonization for *Metrosideros*. An increased genomic sampling within the south Pacific island chains and along the hypothesized origins of the Hawaiian *Metrosideros* (Dupuis et al. 2019; Percy et al. 2008), could clarify the colonization origins and the ancestral diversity of the Hawaiian *Metrosideros*.

Genomic studies of early-stage speciation show that differentiation accumulates in regions that restrict the homogenizing effects of gene flow between incipient species (Feder et al. 2012). The number, size, and distribution of these differentiation outliers can

shed light on the evolutionary factors involved in speciation (Wolf and Ellegren 2017). In *Metrosideros*, the number of outliers did not appear to be associated with the level of gene flow between sister taxa, suggesting that differentiation outliers were not necessarily formed as barriers to gene flow. Spatially, the differentiation outliers were scattered throughout the eleven chromosomes. The phylogenetic sister taxa that were examined for differentiation inhabit contrasting environments [G_{H1} vs. N: wet forest vs. riparian; C vs. I: lower montane vs. low-elevation, dry, including new lava flows; B vs. L: cloud forest vs. upper montane; M vs. T: montane vs. steep windward slope] (Stacy and Sakishima 2019; Dawson and Stemmermann 1990), and differential local adaptation is suggested as the primary driver of their divergence (Morrison and Stacy 2014; Ekar et al. 2019). Combined, these observations suggest that ecological divergence of *Metrosideros* taxa either has a polygenic basis or involves multiple traits with simple genetic architectures. These patterns contrast with the genetic architecture observed for key traits in animal adaptive radiations. For instance, in butterflies (Nadeau et al. 2014), crows (Vijay et al. 2016), and cichlids (Kautt et al. 2020) where adaptive radiation involves different color morphs, few genomic regions are strongly differentiated due to the simple genetic architecture of color-based traits, which also contribute to assortative mating and further builds up differentiation (Servedio et al. 2011). In animal adaptive radiations, in general, differentiation is seemingly localized to a few genomic regions with prominent, broad peaks (Poelstra et al. 2014; Malinsky et al. 2015; Lamichhaney et al. 2015). Unlike in animals, the outlier peaks in *Metrosideros* were narrow and distribution was highly heterogeneous across the genome, a pattern that was also found in the continent-wide adaptive radiation of sunflowers (Renaut et al. 2013). The narrow peaks suggest that homing in on the genes underlying divergent phenotypes may be possible. Further dissection of the genetic architecture of the polygenic ecological traits, however, will require approaches such as GWAS with polygenic risk scores (Fuller et al. 2020) or examination of the underlying gene regulatory networks (Mack and Nachman 2017).

Differentiation outliers can also form from evolutionary factors unrelated to speciation, such as linkage effects from recurrent background selection or selective sweeps on shared genomic features (Burri 2017; Ravinet et al. 2017). The differentiation outliers in *Metrosideros* showed evidence of selective sweeps in multiple taxa, suggesting

that the outlier regions were targets of recurrent selection. Under recurrent sweeps, however, D_{xy} levels of outliers are expected to be lower than those of the genomic background (Cruickshank and Hahn 2014); yet D_{xy} levels of outlier regions in *Metrosideros* were significantly elevated. Elevated D_{xy} were even seen in comparison with a population from the oldest island of Kauai, suggesting that the outlier regions were involved in ancient barriers to gene flow in the common ancestor or that these regions harbor ancient divergent haplotypes that predate colonization of the islands (Han et al. 2017). Long-term balancing selection could have maintained the increased D_{xy} within differentiation outlier regions as taxa radiated across the island (Koenig et al. 2019). Functionally, the enrichment of GO relating to immunity responses for genes within the differentiation outlier regions is consistent with the hypothesis that island-wide shared balancing selection is driving the formation of differentiation outliers in *Metrosideros*.

Our analysis also focused on differentiation outliers that were lineage specific and likely shaped by taxon-specific divergent selection. These lineage-specific accentuated differentiation regions were also enriched for ancient variations, indicating that both historical and contemporary diversification within *Metrosideros* involved selection on ancient divergent haplotypes. Several adaptive radiations have been shown to be facilitated by genetic variations that are older than the radiations themselves (Berner and Salzburger 2015; Marques et al. 2019). Selection on ancient variations may be a common evolutionary mechanism for both animals and plants during adaptive radiation, and may explain how in remote islands with limited gene pools lineages are able to repeatedly radiate into new species (Martin and Richards 2019). Utilizing old variations may explain how different *Metrosideros* taxa have repeatedly colonized similar environments throughout the archipelago, either through selection on standing ancestral variations (Brawand et al. 2014; Pease et al. 2016) or through admixture of ancient divergent haplotypes among hybridizing taxa (Lamichhaney et al. 2015). It may also explain how *Metrosideros* as a long-lived tree has been able to rapidly and repeatedly colonize novel environments.

Materials and Methods

Plant material for the reference genome. About 25 g of young leaves were collected from a mature individual of *M. polymorpha* var. *incana* (NG4) maintained in a coldframe at the University of Hawaii Hilo. NG4 was produced through a controlled-cross between two trees of this variety occurring along Kuliouou Trail, Oahu (approximate location: 21.3160, -157.7296). Leaf material was collected in small batches, wrapped in aluminum foil, and submerged in liquid N_2 within one minute of collection. The bundled samples were then kept at -80C for 72 hours and shipped overnight on dry ice to Oxford Nanopore Technologies, New York, NY and stored again at -80C. The entire tree was covered in a black plastic bag (dark-treated) for 24 hours prior to collection.

Nanopore sequencing-based whole-genome-, RNA-, and Pore-C sequencing. Using the Qiagen DNeasy Plant Mini Kit, DNA was extracted from 2 g of collected leaf tissue. Separately, total RNA was extracted from 1 g of collected leaf tissue using Thermofisher's PureLink RNA Mini Kit. Full-length cDNA was synthesized from 50 ng of total RNA using the Oxford Nanopore Technologies PCS109 kit, followed by 14 rounds of PCR amplification using the primer mixture from the Oxford Nanopore Technologies EXP-PCA001 kit. A detailed protocol outlining the Pore-C method can be found in the Supplemental Text.

A sequencing library was prepared using the Oxford Nanopore Technologies standard ligation sequencing kit SQK-LSK109. Sequencing was conducted on a GridION X5 sequencer for 72 hours, and the raw data were base-called by Oxford Nanopore Technologies basecaller Guppy (available on https://community.nanoporetech.com/) ver. 3.2.8 for the genomic DNA and Pore-C DNA and ver. 3.2.10 for the cDNA in the high-accuracy mode.

Nanopore sequence-based reference genome assembly. The FASTQ files from the whole-genome sequencing data were filtered for high-quality long reads. We used the program filtlong (https://github.com/rrwick/Filtlong) with parameters --min_length 10000 --min_mean_q 85 --min_window_q 70, which selects for reads longer than 10 kbp, average Q-score greater than 8.2, and a minimum sliding window Q-score of 5.2. The

filtered nanopore reads were then assembled with the genome assembler flye (Kolmogorov et al. 2019).

Assembly contig scaffolding with Pore-C sequencing data. The Pore-C data analysis was conducted using the Pore-C workflow developed by Oxford Nanopore Technologies (https://github.com/nanoporetech/Pore-C-Snakemake), which uses the snakemake workflow engine (Köster and Rahmann 2012). Briefly, the workflow first aligns the nanopore Pore-C chromosome contact sequence reads to the unscaffolded *Metrosideros* genome assembly using bwa-sw ver. 0.7.17-r1188 (Li 2013) with parameters -b 5 -q 2 -r 1 -T 15 -z 10. Compared to conventional Hi-C data, Pore-C contains an enrichment of higher order contacts (Ulahannan et al. 2019),and to process the multi-contact nanopore reads we used Pore-C tools (https://github.com/nanoporetech/pore-c) also developed by Oxford Nanopore Technologies. The alignment BAM file was processed with Pore-C tool to filter spurious alignments, detect ligation junctions, and assign fragments that originated from the same chromosomal contacts. Pore-C tools converted the alignment BAM file to a chromosome contact pairs format (https://github.com/4dn-dcic/pairix/blob/master/pairs_format_specification.md) for compatibility with the conventional downstream chromosome contact based analysis methods. The pairs file was converted to a hic file format using the Juicer ver. 1.14.08 tools (Durand et al. 2016b) to use as the input data for the Juicebox assembly tools (Durand et al. 2016a). The Juicebox tools were used to scaffold the draft *Metrosideros* assembly, and we followed established guidelines (https://github.com/theaidenlab/Genome-Assembly-Cookbook) to manually construct the chromosome-scale scaffolds using the Pore-C based chromosome contact frequency information. We assigned chromosome numbers to the superscaffold through synteny with the *Eucalyptus grandis* genome assembly (Myburg et al. 2014). Synteny between the *Metrosideros* superscaffold and *Eucalyptus* chromosomes was determined by aligning the assemblies to each other and visualizing the alignment through the program D-GENIES (Cabanettes and Klopp 2018).

Genome annotation. The cDNA library that was sequenced on the nanopore sequencer was used to annotate the coding sequence regions for the *M. polymorpha* genome

assembly. Initially, we used Pychopper ver. 2.3.1 (https://github.com/nanoporetech/pychopper) to trim primers, identify full-length cDNA sequences, and orient the sequence to the correct strand. A total of 12,298,201 (70.2%) reads were classified by Pychopper and were used for downstream analysis. The long reads were aligned to the reference genome using minimap2 ver. 2.17-r941 (Li 2018) with options -ax splice -uf -k14. The alignment file was then used by stringtie2 ver. 2.1.3b (Kovaka et al. 2019), which is optimized for *de novo* transcriptome assembly using long-read sequencing and a reference genome. We used the MAKER program (Cantarel et al. 2008) for gene annotation using the workflow outlined on the website https://gist.github.com/darencard/bb1001ac1532dd4225b030cf0cd61ce2. The transcriptome assembly from stringtie2 was used as EST evidence in MAKER, and the protein sequences from the previous *M. polymorpha* assembly (Izuno et al. 2019), *E. grandis* assembly (Myburg et al. 2014), and *A. thaliana* (TAIR10) were used for a protein homology search in MAKER. After an initial round of MAKER annotation the gene models were used by SNAP (Korf 2004) and Augustus (Stanke et al. 2008) to create gene model training datasets specifically for our *M. polymorpha* genome assembly. The training dataset was used for a second round of MAKER gene annotation.

We identified the repetitive regions of the *M. polymorpha* reference genome, first using Repeatmodeler ver. 1.0.10 (http://www.repeatmasker.org/RepeatModeler/) for the *de novo* identification repeat sequences in the reference genome, and then using Repeatmasker ver. 4.1.0 (http://www.repeatmasker.org/RepeatMasker/) to identify the genomic locations of the repetitive sequences in our reference genome.

***Metrosideros* population sequencing.** For the population genomic sampling, we collected young leaf tissue from 9-11 adults from each of eight taxa on the focal island of Oahu and fewer adults of two taxa on Kauai. Collected leaf tissue was kept cool and stored at -80C within 48 hours of collection. Leaf material from the three outgroup samples was silica-dried in the field and stored in a dessicator jar. DNA was extracted from both frozen and dried leaf samples using the Macherey-Nagel NucleoSpin Plant II Mini kit. We used a Tn5 transposase-based method to prepare the whole-genome sequencing library. Mosaic End adaptor A and B (Tn5ME-A:

TCGTCGGCAGCGTCAGATGTGTAT AAGAGACAG; Tn5ME-B: GTCTCGTGGGCTCGGAGATGTGTATAAGAGACAG) was annealed with Rev (Tn5ME-Rev: /5Phos/CTGTCTCTTATACACATCT) by mixing 10uL (100uM) of each oligonucleotide with 80 uL of reassociation buffer (10 mM Tris pH 8.0, 50 mM NaCl, 1 mM EDTA) in BioRad thermocycler with the following program: 95°C for 10 min, 90°C for 1 min, and decrease temperature by 1°C/cycle for 60 cycles, held for 1 min at each temperature. Pre-charge of Tn5 with adapters was carried out in solution by mixing 22.5 uL of 100 ng/uL Tn5 (Tn5 protein was produced following the protocol described by (Picelli et al. 2014)), 76.5 uL reassociation buffer/glycerol (1:1), and 4.5 uL of equal molar of annealed adaptor 1 (A-Rev) and annealed adapter 2 (B-Rev). The reaction was then incubated at 37°C for 30 min. The annealed adapters bind to Tn5 transposase to form the transposome complex.

Genomic DNA was tagmented by mixing with 1 uL of the above assembled Tn5 transposome, 4 uL of 5 X TAPS buffer (50 mM TAPS-NaOH pH 8.5 [Alfa aesar # J63268], 25 mM MgCl2, 50% v/dimethylformamide [ThermoFisher #20673], pH 8.5 at 25°C) and water to a total volume of 20 uL and incubated at 55°C for 7 min. The transposome fragments and attaches adapters to gDNA. The reaction was completed by adding 5 uL of 0.2% SDS (Promega, #V6551) to each reaction followed by incubation at 55°C for 7 min to inactivate and release the Tn5. To enrich the DNA fragments that have adapter molecules on both ends we attached an index to the library: 2µl of the stopped tagmentation, 1µl i5 index primer (1uM), 1µl i7 index primer (1µM), 10µl of OneTaq HS Quick-Load 2x master mix (NEB #M0486L), and 6µl of water were combined to make a 20-ul final reaction. The reaction was heated at 68°C for 3min and 95°C for 30 sec, then thermocycled 12 times at 95°C for 10 sec, 55°C for 30 sec, and 68°C for 30 sec, followed by a final extension of 5 min at 68°C.

We then pooled the libraries together, taking 5uL from individual libraries. The pooled library was cleaned and size-selected using Agencourt AMPure XP beads (Beckman Coulter, #A63881) at a 0.8:1 (beads: DNA) ratio. The final library was quantified with a Qubit high-sensitivity DNA kit (Invitrogen Q32854) and examined on an Agilent 2100 Bioanalyzer high-sensitivity DNA chip (Agilent p/n# 2938-85004) to observe the library size distribution. The sequencing library was loaded on a NovaSeq

6000 S1 flow cell and sequenced under a 2×150-bp conformation at the Genomics Core Facility within the Lewis-Sigler Institute for Integrative Genomics at Princeton University. The population genomic sequencing data are available from NCBI bioproject ID PRJNA534153, specifically with the SRR identifiers SRR12673403 to SRR12673495.

Calling genome-wide polymorphisms. Raw sequencing reads were downloaded from our previous study (Choi et al. 2020) and combined with the newly generated sequencing data from the current study. From the sequence read archive (SRA) website we downloaded FASTQs with SRR identifiers SRR8943660 to SRR8943653. The sequencing reads were adapter-trimmed and quality-controlled using BBTools (https://jgi.doe.gov/data-and-tools/bbtools/) bbduk program version 37.66 with option: minlen = 25 qtrim = rl trimq = 10 ktrim = r k = 25 mink = 11 hdist = 1 tpe tbo.

Sequencing reads were then aligned to the scaffolded *M. polymorpha* reference genome generated from this study using bwa-mem. PCR duplicate reads were removed using picard version 2.9.0 (http://broadinstitute.github.io/picard/). Genome-wide read coverage statistics were calculated using GATK version 3.8–0 (https://software.broadinstitute.org/gatk/).

We used the GATK HaplotypeCaller engine to call variant sites from the BAM alignment file for each sample. The option –ERC GVCF was used to output the variants in the gVCF format, and the gVCFs of each sample were merged together to allow a multi-sample joint genotype procedure using GATK GenotypeGVCFs engine. Using standard GATK best-practice hard-filter guidelines, the VariantFiltration engine was used to filter out low-quality polymorphisms. In addition, we removed SNPs that were within 5 bp of an INDEL and polymorphic sites that had less than 80% of individuals with a genotype call.

Population relationship analysis. The alignment BAM files were used to analyze the population relationships between samples. We used ANGSD version 0.929 (Korneliussen et al. 2014) and ngsTools (Fumagalli et al. 2014) to analyze the genotype likelihoods of each sample and infer the population relationships using a probabilistic framework. We only analyzed potential variant sites where more than 80% of the individuals had a

genotype, while enforcing a total sequencing coverage filter such that included sites had a minimum of 1/3 the average total sequencing depth (734×) and a maximum of three times the average total sequencing depth (6,613×). To minimize the effect of linkage on inferences on population relationships, polymorphic sites were randomly pruned using a 10-kbp sliding window with a minimum distance of 5 kbp between random sites.

NGSadmix (Skotte et al. 2013) was used to estimate the admixture proportions (K) for each individual. For each of K = 3 to 15, the analysis was repeated 100 times and the run with the highest log-likelihood was chosen. Phylogeny reconstruction was conducted by estimating the pairwise genetic distances between samples using NGSdist (Vieira et al. 2016), and the genetic distances were used by FastME ver. 2.1.5 (Lefort et al. 2015) to build a neighbor-joining tree. Support of the phylogenetic tree was examined by generating 100 bootstrapped datasets using NGSdist.

Investigating reticulate evolutionary history. The genotype call dataset was used to examine the reticulate evolutionary history of *Metrosideros*. We conducted the ABBA-BABA D test (Green et al. 2010; Durand et al. 2011) and f_3 test (Reich et al. 2009) using the R package admixr (Petr et al. 2019), which is based on the ADMIXTOOLS suite (Patterson et al. 2012). Variants were polarized using the high-coverage Fiji sample *M. vitiensis* as the outgroup genome.

Demographic modeling. We used the methods δaδi (Gutenkunst et al. 2009), G-PhoCS (Gronau et al. 2011), and MSMC (Schiffels and Durbin 2014; Schiffels and Wang 2020) to infer the demographic history of Hawaiian *Metrosideros*. For all analyses we used the genotype call dataset.

For δaδi analysis, we initially randomly thinned the dataset picking a SNP every 10 kbp using PLINK ver. 2.0 (Chang et al. 2015). The site frequency spectrum was estimated using the easySFS.py (https://github.com/isaacovercast/easySFS) script while using Fiji *M. vitiensis* as the outgroup genome and polarizing the polymorphic sites. The easySFS.py script was also used to project down the sample size to maximize the number of sites analyzed. The unfolded site frequency spectrum data were used as input for δaδi, and we fit 20 demographic models (Supplemental Figure 9). We optimized the model

parameter estimates using the Nelder-Mead method by randomly perturbing the parameter values for four rounds. The parameter estimates were perturbed threefold, twofold, twofold, and onefold in incremental rounds. Each round the perturbation was conducted for 10, 20, 30, and 40 replicates. Demography parameters were extracted from the round with the highest likelihood. Demographic models were compared using Akaike Information Criteria (AIC) values. The δaδi analysis scripts were based on the study by (Portik et al. 2017).

To prepare our dataset for G-PhoCS analysis we first partitioned our reference genome into 1-kbp loci and determined those that are close to neutrality. Neutral loci were determined by selecting loci that were 5 kb away from a genic sequence, 500 bp away from a repetitive DNA sequence, and at least 10 kbp away from each other. Since G-PhoCS is designed to analyze the variation within a single genome, we selected a single individual with high genome coverage to represent each island. Selected samples included: H207 from Hawaii Island (population G_{H1}), X83 from Molokai (population G_M), O385 from Oahu (taxon M), and K283 from Kauai (population G_K). The *M. vitiensis* sample from Fiji was used as the outgroup. We used G-PhoCS ver. 1.2.3 and ran every demographic model five times to check for convergence in the demographic parameter estimates. Each MCMC run had 1,000,000 iterations, and the initial 500,000 iterations were discarded as burn-in. Priors were modeled using a gamma distribution ($\alpha = 1$ and $\beta = 10{,}000$ for population size and divergence time; $\alpha = 0.002$ and $\beta = 0.00001$ for migration rates). Different demographic models involved fitting migration bands between two terminal lineages. After the MCMC run was complete, the program Tracer version 1.6 (http://tree.bio.ed.ac.uk/software/tracer/) was used to estimate the 95% highest posterior density for each demography parameter. The G-PhoCS-estimated divergence time τ is scaled according to the mutation rate (μ). To convert divergence time to absolute divergence time T (in years) we used the following equation:

$$T = \frac{\tau \times g}{\mu}$$

where g represents the generation time.

MSMC2 was used to estimate the past changes in effective population sizes and the divergence times between individuals. From each taxon/population we chose a single

representative individual for the MSMC2 analysis as follows: O310 (taxon B), O65 (taxon C), O72 (taxon I), O194 (taxon L), H271 (taxon N), O464 (taxon R), O145 (taxon T), plus the individuals used in the G-PhoCS analysis. We used the alignment BAM file for each individual and the mpileup function of samtools ver. 1.3.1 (Li et al. 2009) to detect sites that had a minimum base score of 30, a mapping quality score of 30, and the coefficient to downgrade mapping qualities for excessive mismatches at 50. The resulting text pileup output was used by bcftools ver. 1.3.1 to call variant sites but excluding INDELs and limiting the calls to biallelic SNPs. The bamCaller.py script that was provided by the MSMC suite (https://github.com/stschiff/msmc-tools) was then used to produce the per-chromosome masks and VCF files for each individual. A genome-wide mask file was also created for each individual by using the SNPable workflow (http://lh3lh3.users.sourceforge.net/snpable.shtml) on each superscaffold/chromosome assembly and then converting it to BED format using the makeMappabilityMask.py script within the MSMC suite. Phasing was done by using the output from the beagle analysis. The input files for MSMC2 were generated using the generate_multihetsep.py script, which is also part of the MSMC suite. To estimate changes in effective population size we examined the two haplotypes of each individual, while cross coalescence rates were estimated from four haplotypes from two individuals. The combineCrossCoal.py script from the MSMC suite was used to produce the outputs for plotting.

Population genomic analysis. We used the gVCFs that were called from the previous step to create a VCF file that had genotype calls for all sites including the non-variant positions. The GATK GenotypeGVCFs engine was used with the option –includeNonVariantSites. We analyzed a population VCF that had both variant and non-variant sites in order to obtain the correct number of sites to be used as the denominator for the population genetic statistics we were calculating. We used the genomics_general package to calculate θ, D_{xy}, and F_{ST} in 10 kbp windows, sliding the window by 5 kbp. For each window we imposed a quality filter only analyzing sites that had a minimum quality score of 30 and a minimum depth of 5×. Windows that had more than 30% of the sites with a genotype call after the filter were chosen for downstream analysis.

To search for genomic outliers of differentiation the F_{ST} values were *Z*-transformed (zF_{ST}), and genomic windows with $zF_{ST} \geq 4$ were considered outliers (Han et al. 2017). To search for genomic regions with lineage-specific accentuated differentiation we used a comparative population genomic approach and to avoid analyzing differentiation outlier regions shaped by linked selection effects (Burri 2017). For each phylogenetic sister pair, a zF_{ST} genome scan was conducted, and the zFst value at each 10 kbp window was compared with those for each of the three other sister pairs. Genomic windows for which the focal sister pair had $zF_{ST} \geq 4$ but the other sister pairs had $zF_{ST} < 4$ were considered to be regions of lineage-specific accentuated differentiation. Further, we required at least two consecutive windows with evidence of lineage-specific accentuated differentiation to avoid spurious outliers.

The strength of evidence of selective sweeps was estimated using the ω statistic (Kim and Nielsen 2004). We used the program OmegaPlus (Alachiotis et al. 2012), which is specifically designed to estimate the ω statistics for genome-wide SNP datasets. We set the grid size of OmegaPlus so that the ω statistics would be estimated at 10-kbp windows for each superscaffold/chromosome.

Acknowledgements.

We thank Jennifer Johansen, Yohan Pillon, Melissa Johnson, and Chrissen Gemmill for assistance with field collections, Tomoko Sakishima for assistance with greenhouse sample collection and DNA extractions, the College of Agriculture, Forestry, and Natural Resource Management at the University of Hawaii Hilo for greenhouse space, and Angalee Kirby for greenhouse management, We are also grateful to the Genomics Core Facility at Princeton University for sequencing support and the New York University IT High Performance Computing for supplying the computational resources, services, and staff expertise.

Supplemental Labels

Supplemental Figure 1. Ancestry proportions for K=3 to K=15 across all Hawaiian archipelago samples.

Supplemental Figure 2. ABBA-BABA D-test statistics for all taxa/population trio combinations.

Supplemental Figure 3. G-PhoCS-based divergence time estimates for different migration models.

Supplemental Figure 4. The number of overlapping zF_{ST} outlier positions.

Supplemental Figure 5. Between-taxon/population correlations in sequence diversity (π), divergence (D_{xy}), differentiation (F_{ST}), and selective sweep statistics (ω_{max}).

Supplemental Figure 6. Divergence (D_{xy}) statistics identified in a sister pair (left window) and the same pairwise statistics calculated for the same regions between one member of the pair and 4 other taxa representing increasing genomic divergence (right window). Red boxes are statistics from the genomic background, and green boxes are statistics from the Lineage specific accentuated differentiation outlier regions. * indicate $p < 0.05$, ** indicate $p < 0.01$, and *** indicate $p < 0.001$.

Supplemental Figure 7. Significantly enriched gene ontology terms for genes overlapping genomic regions of differentiation outliers.

Supplemental Table 1. Sequencing statistics from the nanopore sequencing of the whole genome.

Supplemental Table 2. Aggregated Pore-C sequencing and number of contact results.

Supplemental Table 3. Sequencing statistics from the nanopore sequencing of the cDNA library.

Supplemental Table 4. Population sample information.

Supplemental Table 5. δaδi results for all 20 demography models for all 4 sister pairs.

Supplemental Table 6. Coordinates of the lineage-specific accentuated differentiation regions.

References

Alachiotis N, Stamatakis A, Pavlidis P. 2012. OmegaPlus: a scalable tool for rapid detection of selective sweeps in whole-genome datasets. *Bioinformatics* **28**: 2274–2275.

Anacker BL, Strauss SY. 2014. The geography and ecology of plant speciation: range overlap and niche divergence in sister species. *Proceedings of the Royal Society B: Biological Sciences* **281**: 20132980.

Barrier M, Baldwin BG, Robichaux RH, Purugganan MD. 1999. Interspecific hybrid ancestry of a plant adaptive radiation: allopolyploidy of the Hawaiian silversword alliance (Asteraceae) inferred from floral homeotic gene duplications. *Mol Biol Evol* **16**: 1105–1113.

Berner D, Salzburger W. 2015. The genomics of organismal diversification illuminated by adaptive radiations. *Trends Genet* **31**: 491–499.

Brawand D, Wagner CE, Li YI, Malinsky M, Keller I, Fan S, Simakov O, Ng AY, Lim ZW, Bezault E, et al. 2014. The genomic substrate for adaptive radiation in African cichlid fish. *Nature* **513**: 375–381.

Burri R. 2017. Interpreting differentiation landscapes in the light of long-term linked selection. *Evolution Letters* **1**: 118–131.

Burri R, Nater A, Kawakami T, Mugal CF, Olason PI, Smeds L, Suh A, Dutoit L, Bureš S, Garamszegi LZ, et al. 2015. Linked selection and recombination rate variation drive the evolution of the genomic landscape of differentiation across the speciation continuum of Ficedula flycatchers. *Genome Res* gr.196485.115.

Cabanettes F, Klopp C. 2018. D-GENIES: dot plot large genomes in an interactive, efficient and simple way. *PeerJ* **6**. https://www.ncbi.nlm.nih.gov/pmc/articles/PMC5991294/ (Accessed June 12, 2019).

Campbell CR, Poelstra JW, Yoder AD. 2018. What is Speciation Genomics? The roles of ecology, gene flow, and genomic architecture in the formation of species. *Biol J Linn Soc* **124**: 561–583.

Cantarel BL, Korf I, Robb SMC, Parra G, Ross E, Moore B, Holt C, Sánchez Alvarado A, Yandell M. 2008. MAKER: An easy-to-use annotation pipeline designed for emerging model organism genomes. *Genome Res* **18**: 188–196.

Carr GD. 1978. Chromosome Numbers of Hawaiian Flowering Plants and the Significance of Cytology in Selected Taxa. *American Journal of Botany* **65**: 236–242.

Carson HL, Kaneshiro KY. 1976. Drosophila of Hawaii: Systematics and Ecological Genetics. *Annu Rev Ecol Syst* **7**: 311–345.

Chang CC, Chow CC, Tellier LC, Vattikuti S, Purcell SM, Lee JJ. 2015. Second-generation PLINK: rising to the challenge of larger and richer datasets. *Gigascience* **4**. https://academic.oup.com/gigascience/article/4/1/s13742-015-0047-8/2707533 (Accessed June 17, 2020).

Charlesworth B. 1998. Measures of divergence between populations and the effect of forces that reduce variability. *Molecular Biology and Evolution* **15**: 538–543.

Choi JY, Purugganan M, Stacy EA. 2020. Divergent Selection and Primary Gene Flow Shape Incipient Speciation of a Riparian Tree on Hawaii Island. *Mol Biol Evol* **37**: 695–710.

Clague D. 1996. The growth and subsidence of the Hawaiian-Emperor volcanic chain. In *The origin and evolution of Pacific island biotas, New Guinea to eastern Polynesia: patterns and processes*, pp. 35–50, SPB Academic Publishing, Amsterdam, The Netherlands.

Cordell S, Goldstein G, Melcher PJ, Meinzer FC. 2000. Photosynthesis and Freezing Avoidance in Ohia (Metrosideros polymorpha) at Treeline in Hawaii. *Arctic, Antarctic, and Alpine Research* **32**: 381–387.

Cordell S, Goldstein G, Mueller-Dombois D, Webb D, Vitousek PM. 1998. Physiological and morphological variation in Metrosideros polymorpha, a dominant Hawaiian tree species, along an altitudinal gradient: the role of phenotypic plasticity. *Oecologia* **113**: 188–196.

Corn CA, Hiesey WM. 1973. Altitudinal variation in hawaiian metrosideros. *American Journal of Botany* **60**: 991–1002.

Cruickshank TE, Hahn MW. 2014. Reanalysis suggests that genomic islands of speciation are due to reduced diversity, not reduced gene flow. *Molecular Ecology* **23**: 3133–3157.

Dawson J, Stemmermann L. 1990. Metrosideros (Gaud). In *Manual of the flowering plants of Hawai'i* (eds. W. Wagner, D. Herbst, and S. Sohmer), pp. 964–970, Univ. Hawai'i Press, Honolulu, Hawai'i.

Dupuis JR, Pillon Y, Sakishima T, Gemmill CEC, Chamala S, Barbazuk WB, Geib SM, Stacy EA. 2019. Targeted amplicon sequencing of 40 nuclear genes supports a single introduction and rapid radiation of Hawaiian Metrosideros (Myrtaceae). *Plant Syst Evol*. https://doi.org/10.1007/s00606-019-01615-0 (Accessed October 7, 2019).

Durand EY, Patterson N, Reich D, Slatkin M. 2011. Testing for Ancient Admixture between Closely Related Populations. *Molecular Biology and Evolution* **28**: 2239–2252.

Durand NC, Robinson JT, Shamim MS, Machol I, Mesirov JP, Lander ES, Aiden EL. 2016a. Juicebox Provides a Visualization System for Hi-C Contact Maps with Unlimited Zoom. *Cell Syst* **3**: 99–101.

Durand NC, Shamim MS, Machol I, Rao SSP, Huntley MH, Lander ES, Aiden EL. 2016b. Juicer Provides a One-Click System for Analyzing Loop-Resolution Hi-C Experiments. *cels* **3**: 95–98.

Ekar JM, Price DK, Johnson MA, Stacy EA. 2019. Varieties of the highly dispersible and hypervariable tree, Metrosideros polymorpha, differ in response to mechanical stress and light across a sharp ecotone. *Am J Bot* **106**: 1106–1115.

Feder JL, Egan SP, Nosil P. 2012. The genomics of speciation-with-gene-flow. *Trends in Genetics* **28**: 342–350.

Frankham R. 1997. Do island populations have less genetic variation than mainland populations? *Heredity (Edinb)* **78 (Pt 3)**: 311–327.

Fuller ZL, Mocellin VJL, Morris LA, Cantin N, Shepherd J, Sarre L, Peng J, Liao Y, Pickrell J, Andolfatto P, et al. 2020. Population genetics of the coral Acropora millepora: Toward genomic prediction of bleaching. *Science* **369**. https://science.sciencemag.org/content/369/6501/eaba4674 (Accessed October 30, 2020).

Fumagalli M, Vieira FG, Linderoth T, Nielsen R. 2014. ngsTools: methods for population genetics analyses from next-generation sequencing data. *Bioinformatics* **30**: 1486–7.

Futuyma DJ. 1998. *Evolutionary Biology*. Sinauer Associates.

Gillespie RG, Bennett GM, De Meester L, Feder JL, Fleischer RC, Harmon LJ, Hendry AP, Knope ML, Mallet J, Martin C, et al. 2020. Comparing Adaptive Radiations Across Space, Time, and Taxa. *J Hered* **111**: 1–20.

Givnish T. 1997. Adaptive radiations and molecular systematics: issues and approaches. In *Molecular Evolution and Adaptive Radiation*, (eds. T. Givnish and K. Sytsma), pp. 1–54, Cambridge Univ. Press, Cambridge, UK.

Givnish TJ. 2015. Adaptive radiation versus “radiation” and “explosive diversification”: why conceptual distinctions are fundamental to understanding evolution. *New Phytol* **207**: 297–303.

Givnish TJ, Millam KC, Mast AR, Paterson TB, Theim TJ, Hipp AL, Henss JM, Smith JF, Wood KR, Sytsma KJ. 2009. Origin, adaptive radiation and diversification of the Hawaiian lobeliads (Asterales: Campanulaceae). *Proceedings of the Royal Society B: Biological Sciences* **276**: 407–416.

Glor RE. 2010. Phylogenetic Insights on Adaptive Radiation. *Annual Review of Ecology, Evolution, and Systematics* **41**: 251–270.

Grant PR, Grant BR. 2008. *How and why species multiply: The Radiations of Darwin’s Finches*. Princeton University Press, Princeton, NJ.

Green RE, Krause J, Briggs AW, Maricic T, Stenzel U, Kircher M, Patterson N, Li H, Zhai W, Fritz MH-Y, et al. 2010. A draft sequence of the Neandertal genome. *Science* **328**: 710–22.

Gronau I, Hubisz MJ, Gulko B, Danko CG, Siepel A. 2011. Bayesian inference of ancient human demography from individual genome sequences. *Nat Genet* **43**: 1031–1034.

Gutenkunst RN, Hernandez RD, Williamson SH, Bustamante CD. 2009. Inferring the joint demographic history of multiple populations from multidimensional SNP frequency data. *PLoS Genet* **5**: e1000695.

Han F, Lamichhaney S, Grant BR, Grant PR, Andersson L, Webster MT. 2017. Gene flow, ancient polymorphism, and ecological adaptation shape the genomic landscape of divergence among Darwin’s finches. *Genome research* **27**: 1004–1015.

Hart PJ. 2010. Tree growth and age in an ancient Hawaiian wet forest: vegetation dynamics at two spatial scales. *Journal of Tropical Ecology* **26**: 1–11.

Izuno A, Wicker T, Hatakeyama M, Copetti D, Shimizu KK. 2019. Updated Genome Assembly and Annotation for Metrosideros polymorpha, an Emerging Model Tree Species of Ecological Divergence. *G3: Genes, Genomes, Genetics* **9**: 3513–3520.

Kaplan N, Dekker J. 2013. High-throughput genome scaffolding from in vivo DNA interaction frequency. *Nature Biotechnology* **31**: 1143–1147.

Kautt AF, Kratochwil CF, Nater A, Machado-Schiaffino G, Olave M, Henning F, Torres-Dowdall J, Härer A, Hulsey CD, Franchini P, et al. 2020. Contrasting signatures of genomic divergence during sympatric speciation. *Nature* 1–6.

Kim Y, Nielsen R. 2004. Linkage disequilibrium as a signature of selective sweeps. *Genetics* **167**: 1513–24.

Kitayama K, Pattison R, Cordell S, Webb D, Mueller-Dombois D. 1997. Ecological and Genetic Implications of Foliar Polymorphism in Metrosideros polymorpha Gaud. (Myrtaceae) in a Habitat Matrix on Mauna Loa, Hawaii. *Ann Bot* **80**: 491–497.

Koenig D, Hagmann J, Li R, Bemm F, Slotte T, Neuffer B, Wright SI, Weigel D. 2019. Long-term balancing selection drives evolution of immunity genes in Capsella eds. M. Przeworski, I.T. Baldwin, and Z. Gao. *eLife* **8**: e43606.

Kolmogorov M, Yuan J, Lin Y, Pevzner PA. 2019. Assembly of long, error-prone reads using repeat graphs. *Nature Biotechnology* **37**: 540.

Korf I. 2004. Gene finding in novel genomes. *BMC Bioinformatics* **5**: 59.

Korneliussen TS, Albrechtsen A, Nielsen R. 2014. ANGSD: Analysis of Next Generation Sequencing Data. *BMC bioinformatics* **15**: 356.

Köster J, Rahmann S. 2012. Snakemake—a scalable bioinformatics workflow engine. *Bioinformatics* **28**: 2520–2522.

Kovaka S, Zimin AV, Pertea GM, Razaghi R, Salzberg SL, Pertea M. 2019. Transcriptome assembly from long-read RNA-seq alignments with StringTie2. *Genome Biology* **20**: 278.

Lamichhaney S, Berglund J, Almén MS, Maqbool K, Grabherr M, Martinez-Barrio A, Promerová M, Rubin C-J, Wang C, Zamani N, et al. 2015. Evolution of Darwin's finches and their beaks revealed by genome sequencing. *Nature* **518**: 371–375.

Lefort V, Desper R, Gascuel O. 2015. FastME 2.0: A Comprehensive, Accurate, and Fast Distance-Based Phylogeny Inference Program. *Molecular Biology and Evolution* **32**: 2798–2800.

Li H. 2013. Aligning sequence reads, clone sequences and assembly contigs with BWA-MEM. *arXiv* 1303.3997v2.

Li H. 2018. Minimap2: pairwise alignment for nucleotide sequences. *Bioinformatics* **34**: 3094–3100.

Li H, Handsaker B, Wysoker A, Fennell T, Ruan J, Homer N, Marth G, Abecasis G, Durbin R, 1000 Genome Project Data Processing Subgroup. 2009. The Sequence Alignment/Map format and SAMtools. *Bioinformatics* **25**: 2078–2079.

Losos J. 2009. *Lizards in an Evolutionary Tree: Ecology and Adaptive Radiation of Anoles*. University of California Press.

Losos JB. 2010. Adaptive radiation, ecological opportunity, and evolutionary determinism. American Society of Naturalists E. O. Wilson award address. *Am Nat* **175**: 623–639.

Losos JB, Ricklefs RE. 2009. Adaptation and diversification on islands. *Nature* **457**: 830–836.

Mack KL, Nachman MW. 2017. Gene Regulation and Speciation. *Trends Genet* **33**: 68–80.

Malinsky M, Challis RJ, Tyers AM, Schiffels S, Terai Y, Ngatunga BP, Miska EA, Durbin R, Genner MJ, Turner GF. 2015. Genomic islands of speciation separate cichlid ecomorphs in an East African crater lake. *Science* **350**: 1493–1498.

Mallet J. 2007. Hybrid speciation. *Nature* **446**: 279–283.

Marques DA, Meier JI, Seehausen O. 2019. A Combinatorial View on Speciation and Adaptive Radiation. *Trends Ecol Evol (Amst)* **34**: 531–544.

Martin CH, Richards EJ. 2019. The Paradox Behind the Pattern of Rapid Adaptive Radiation: How Can the Speciation Process Sustain Itself Through an Early Burst? *Annual Review of Ecology, Evolution, and Systematics* **50**: 569–593.

Morrison KR, Stacy EA. 2014. Intraspecific divergence and evolution of a life-history trade-off along a successional gradient in Hawaii's Metrosideros polymorpha. *Journal of Evolutionary Biology* **27**: 1192–1204.

Myburg AA, Grattapaglia D, Tuskan GA, Hellsten U, Hayes RD, Grimwood J, Jenkins J, Lindquist E, Tice H, Bauer D, et al. 2014. The genome of Eucalyptus grandis. *Nature* **510**: 356–362.

Nachman MW, Payseur BA. 2012. Recombination rate variation and speciation: theoretical predictions and empirical results from rabbits and mice. *Philos Trans R Soc Lond B Biol Sci* **367**: 409–421.

Nadeau NJ, Ruiz M, Salazar P, Counterman B, Medina JA, Ortiz-Zuazaga H, Morrison A, McMillan WO, Jiggins CD, Papa R. 2014. Population genomics of parallel hybrid zones in the mimetic butterflies, H. melpomene and H. erato. *Genome Res* **24**: 1316–1333.

Nevado B, Wong ELY, Osborne OG, Filatov DA. 2019. Adaptive Evolution Is Common in Rapid Evolutionary Radiations. *Curr Biol* **29**: 3081-3086.e5.

Noor M a. F, Bennett SM. 2009. Islands of speciation or mirages in the desert? Examining the role of restricted recombination in maintaining species. *Heredity* **103**: 439–444.

Olson ME, Arroyo-Santos A. 2009. Thinking in continua: beyond the "adaptive radiation" metaphor. *Bioessays* **31**: 1337–1346.

Patterson N, Moorjani P, Luo Y, Mallick S, Rohland N, Zhan Y, Genschoreck T, Webster T, Reich D. 2012. Ancient Admixture in Human History. *Genetics* **192**: 1065–1093.

Pease JB, Haak DC, Hahn MW, Moyle LC. 2016. Phylogenomics Reveals Three Sources of Adaptive Variation during a Rapid Radiation. *PLOS Biology* **14**: e1002379.

Percy DM, Garver AM, Wagner WL, James HF, Cunningham CW, Miller SE, Fleischer RC. 2008. Progressive island colonization and ancient origin of Hawaiian Metrosideros (Myrtaceae). *Proceedings Biological sciences* **275**: 1479–90.

Petr M, Vernot B, Kelso J. 2019. admixr—R package for reproducible analyses using ADMIXTOOLS. *Bioinformatics* **35**: 3194–3195.

Picelli S, Björklund ÅK, Reinius B, Sagasser S, Winberg G, Sandberg R. 2014. Tn5 transposase and tagmentation procedures for massively scaled sequencing projects. *Genome Res* **24**: 2033–2040.

Poelstra JW, Vijay N, Bossu CM, Lantz H, Ryll B, Müller I, Baglione V, Unneberg P, Wikelski M, Grabherr MG, et al. 2014. The genomic landscape underlying phenotypic integrity in the face of gene flow in crows. *Science* **344**: 1410–1414.

Portik DM, Leaché AD, Rivera D, Barej MF, Burger M, Hirschfeld M, Rödel M-O, Blackburn DC, Fujita MK. 2017. Evaluating mechanisms of diversification in a Guineo-Congolian tropical forest frog using demographic model selection. *Molecular Ecology* **26**: 5245–5263.

Price JP, Clague DA. 2002. How old is the Hawaiian biota? Geology and phylogeny suggest recent divergence. *Proceedings of the Royal Society of London Series B: Biological Sciences* **269**: 2429–2435.

Ravinet M, Faria R, Butlin RK, Galindo J, Bierne N, Rafajlović M, Noor MAF, Mehlig B, Westram AM. 2017. Interpreting the genomic landscape of speciation: a road map for finding barriers to gene flow. *Journal of Evolutionary Biology* **30**: 1450–1477.

Reich D, Thangaraj K, Patterson N, Price AL, Singh L. 2009. Reconstructing Indian population history. *Nature* **461**: 489–94.

Renaut S, Grassa CJ, Yeaman S, Moyers BT, Lai Z, Kane NC, Bowers JE, Burke JM, Rieseberg LH. 2013. Genomic islands of divergence are not affected by geography of speciation in sunflowers. *Nature Communications* **4**: 1–8.

Richards EJ, Servedio MR, Martin CH. 2019. Searching for Sympatric Speciation in the Genomic Era. *BioEssays* **41**: 1900047.

Robichaux RH, Carr GD, Liebman M, Pearcy RW. 1990. Adaptive Radiation of the Hawaiian Silversword Alliance (Compositae- Madiinae): Ecological, Morphological, and Physiological Diversity. *Annals of the Missouri Botanical Garden* **77**: 64–72.

Rundle HD, Nosil P. 2005. Ecological speciation. *Ecology Letters* **8**: 336–352.

Schiffels S, Durbin R. 2014. Inferring human population size and separation history from multiple genome sequences. *Nature Genetics* **46**: 919–925.

Schiffels S, Wang K. 2020. MSMC and MSMC2: The Multiple Sequentially Markovian Coalescent. In *Statistical Population Genomics* (ed. J.Y. Dutheil), *Methods in Molecular Biology*, pp. 147–166, Springer US, New York, NY https://doi.org/10.1007/978-1-0716-0199-0_7 (Accessed August 22, 2020).

Schluter D. 2009. Evidence for ecological speciation and its alternative. *Science* **323**: 737–41.

Schluter D. 2000. *The Ecology of Adaptive Radiation*. Oxford University Press.

Seehausen O, Butlin RK, Keller I, Wagner CE, Boughman JW, Hohenlohe PA, Peichel CL, Saetre G-P, Bank C, Brännström Å, et al. 2014. Genomics and the origin of species. *Nature Reviews Genetics* **15**: 176–192.

Servedio MR, Doorn GSV, Kopp M, Frame AM, Nosil P. 2011. Magic traits in speciation: 'magic' but not rare? *Trends in Ecology & Evolution* **26**: 389–397.

Shaw KL, Gillespie RG. 2016. Comparative phylogeography of oceanic archipelagos: Hotspots for inferences of evolutionary process. *Proc Natl Acad Sci U S A* **113**: 7986–7993.

Simpson GG. 1944. *Tempo and Mode in Evolution*. Columbia University Press.

Simpson GG. 1953. *The Major Features of Evolution*. Columbia University Press.

Skotte L, Korneliussen TS, Albrechtsen A. 2013. Estimating Individual Admixture Proportions from Next Generation Sequencing Data. *Genetics* **195**: 693–702.

Stacy EA, Johansen JB, Sakishima T, Price DK. 2016. Genetic analysis of an ephemeral intraspecific hybrid zone in the hypervariable tree, Metrosideros polymorpha, on Hawai'i Island. *Heredity* **117**: 173–183.

Stacy EA, Johansen JB, Sakishima T, Price DK, Pillon Y. 2014. Incipient radiation within the dominant Hawaiian tree Metrosideros polymorpha. *Heredity* **113**: 334–342.

Stacy EA, Sakishima T. 2019. Phylogeography of the highly dispersible landscape-dominant woody species complex, Metrosideros, in Hawaii. *Journal of Biogeography* **46**: 2215–2231.

Stacy EA, Sakishima T, Tharp H, Snow N. 2020. Isolation of Metrosideros ('Ohi'a) Taxa on O'ahu Increases with Elevation and Extreme Environments. *J Hered* **111**: 103–118.

Stanke M, Diekhans M, Baertsch R, Haussler D. 2008. Using native and syntenically mapped cDNA alignments to improve de novo gene finding. *Bioinformatics* **24**: 637–644.

Stankowski S, Chase MA, Fuiten AM, Rodrigues MF, Ralph PL, Streisfeld MA. 2019. Widespread selection and gene flow shape the genomic landscape during a radiation of monkeyflowers. *PLOS Biology* **17**: e3000391.

Stemmermann L. 1983. Ecological studies of Hawaiian Metrosideros in a successional context. *Pacific Science* **37**: 361–373.

Sur GL, Keating R, Snow N, Stacy EA. 2018. Leaf Micromorphology Aids Taxonomic Delineation within the Hypervariable Genus Metrosideros (Myrtaceae) on O'ahu. *pasc* **72**: 345–361.

Tsujii Y, Onoda Y, Izuno A, Isagi Y, Kitayama K. 2016. A quantitative analysis of phenotypic variations of Metrosideros polymorpha within and across populations along environmental gradients on Mauna Loa, Hawaii. *Oecologia* **180**: 1049–1059.

Ulahannan N, Pendleton M, Deshpande A, Schwenk S, Behr JM, Dai X, Tyer C, Rughani P, Kudman S, Adney E, et al. 2019. Nanopore sequencing of DNA concatemers reveals higher-order features of chromatin structure. *bioRxiv* 833590.

Via S. 2009. Natural selection in action during speciation. *PNAS* **106**: 9939–9946.

Vieira FG, Lassalle F, Korneliussen TS, Fumagalli M. 2016. Improving the estimation of genetic distances from Next-Generation Sequencing data. *Biological Journal of the Linnean Society* **117**: 139–149.

Vijay N, Bossu CM, Poelstra JW, Weissensteiner MH, Suh A, Kryukov AP, Wolf JBW. 2016. Evolution of heterogeneous genome differentiation across multiple contact zones in a crow species complex. *Nature Communications* **7**: 13195.

Wagner WL, Funk VA. 1995. *Hawaiian biogeography: evolution on a hotspot archipelago*. Smithsonian Institution Press, Washington, DC.

Wilson EO. 1992. *The Diversity of Life*. Harvard University Press.

Wolf JBW, Ellegren H. 2017. Making sense of genomic islands of differentiation in light of speciation. *Nature Reviews Genetics* **18**: 87–100.

A

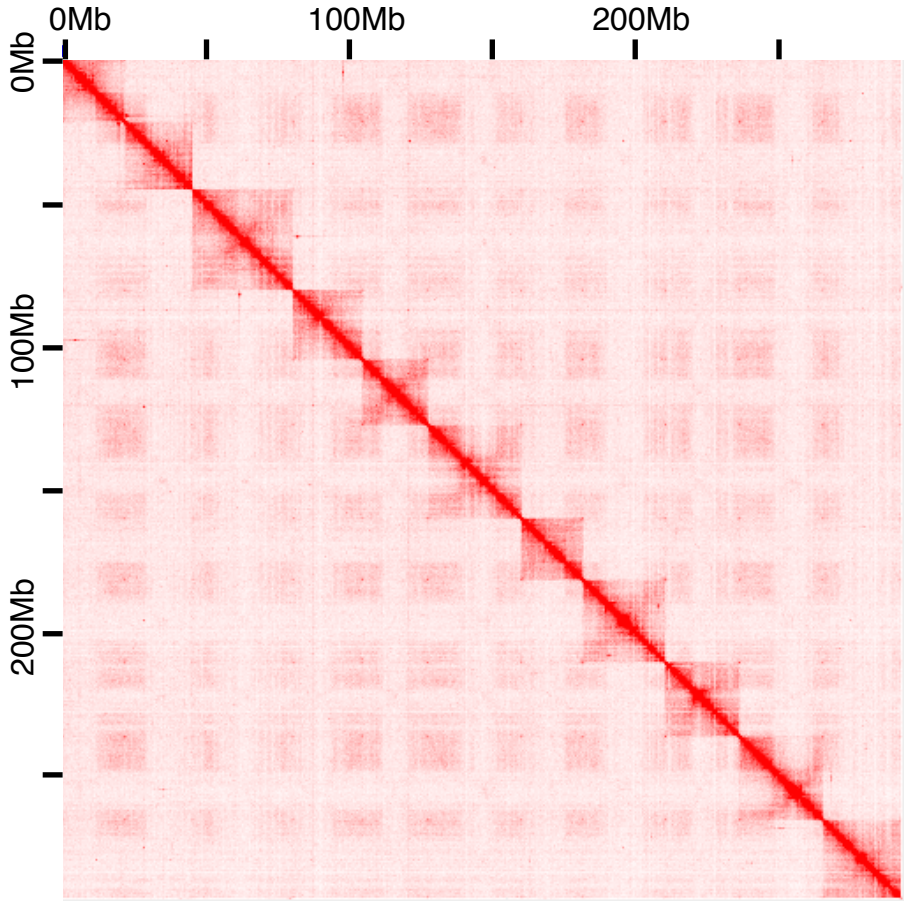
0Mb
100Mb
200Mb
0Mb
100Mb
200Mb

B

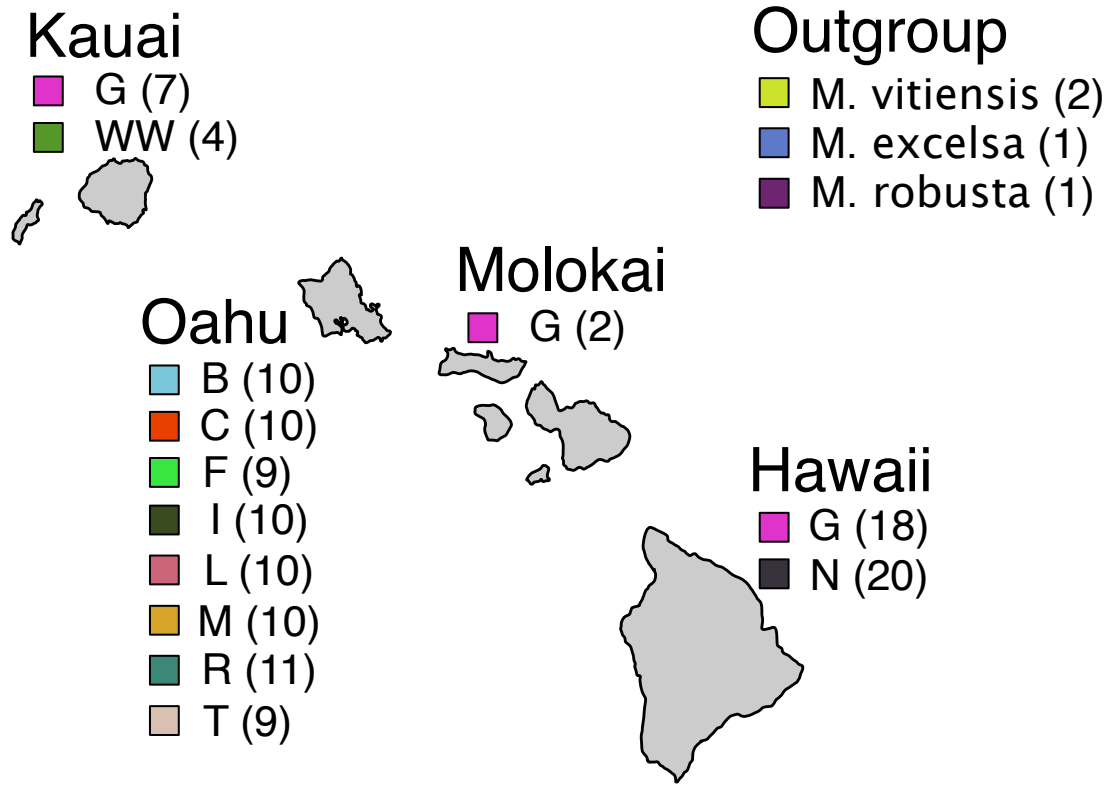
Kauai
G (7)
WW (4)
Outgroup
M. vitiensis (2)
M. excelsa (1)
M. robusta (1)
Oahu
B (10)
C (10)
F (9)
I (10)
L (10)
M (10)
R (11)
T (9)
Molokai
G (2)
Hawaii
G (18)
N (20)

C

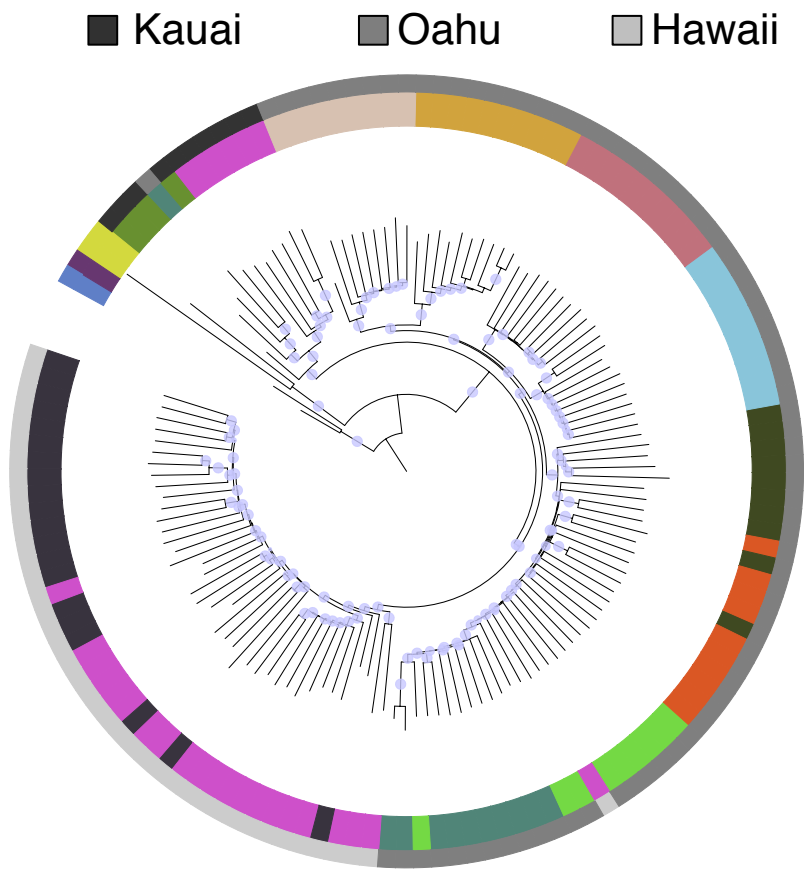
Kauai
Oahu
Hawaii

D

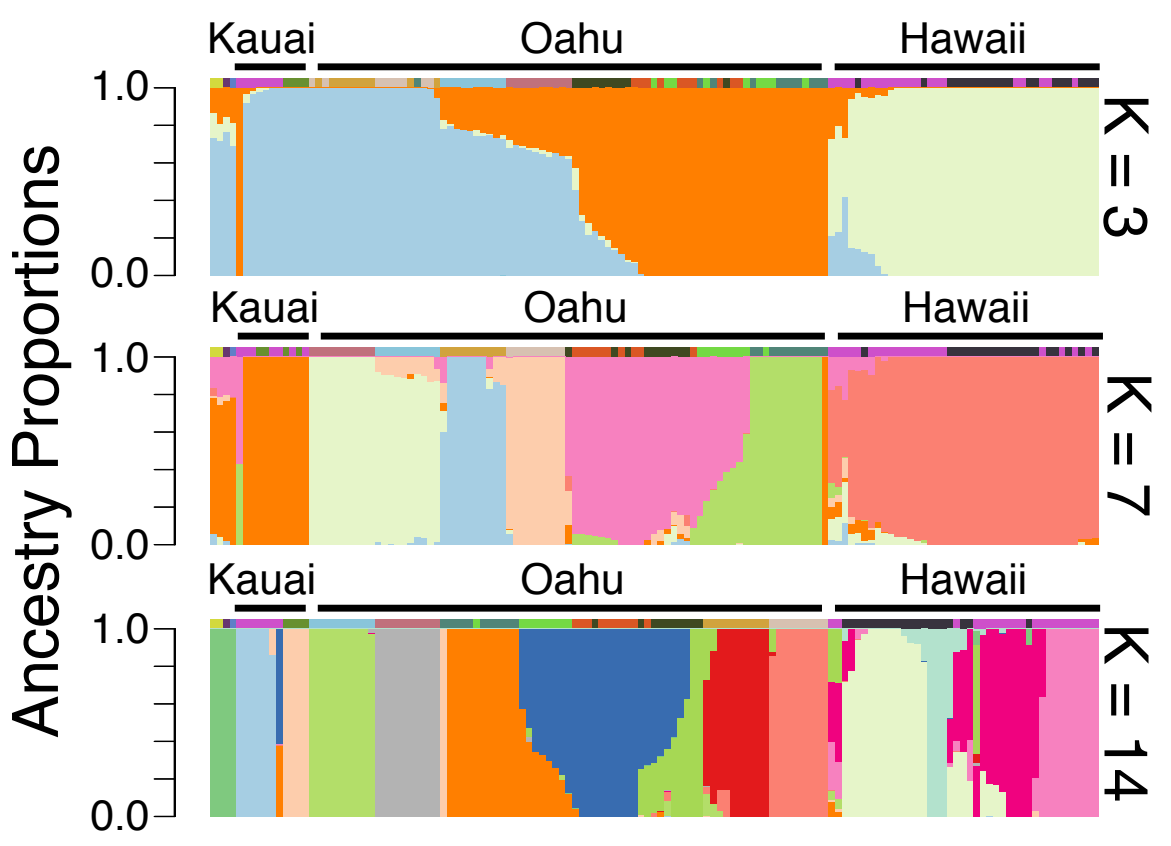
Ancestry Proportions
Kauai
Oahu
Hawaii
1.0
0.0
K = 3
K = 7
K = 14

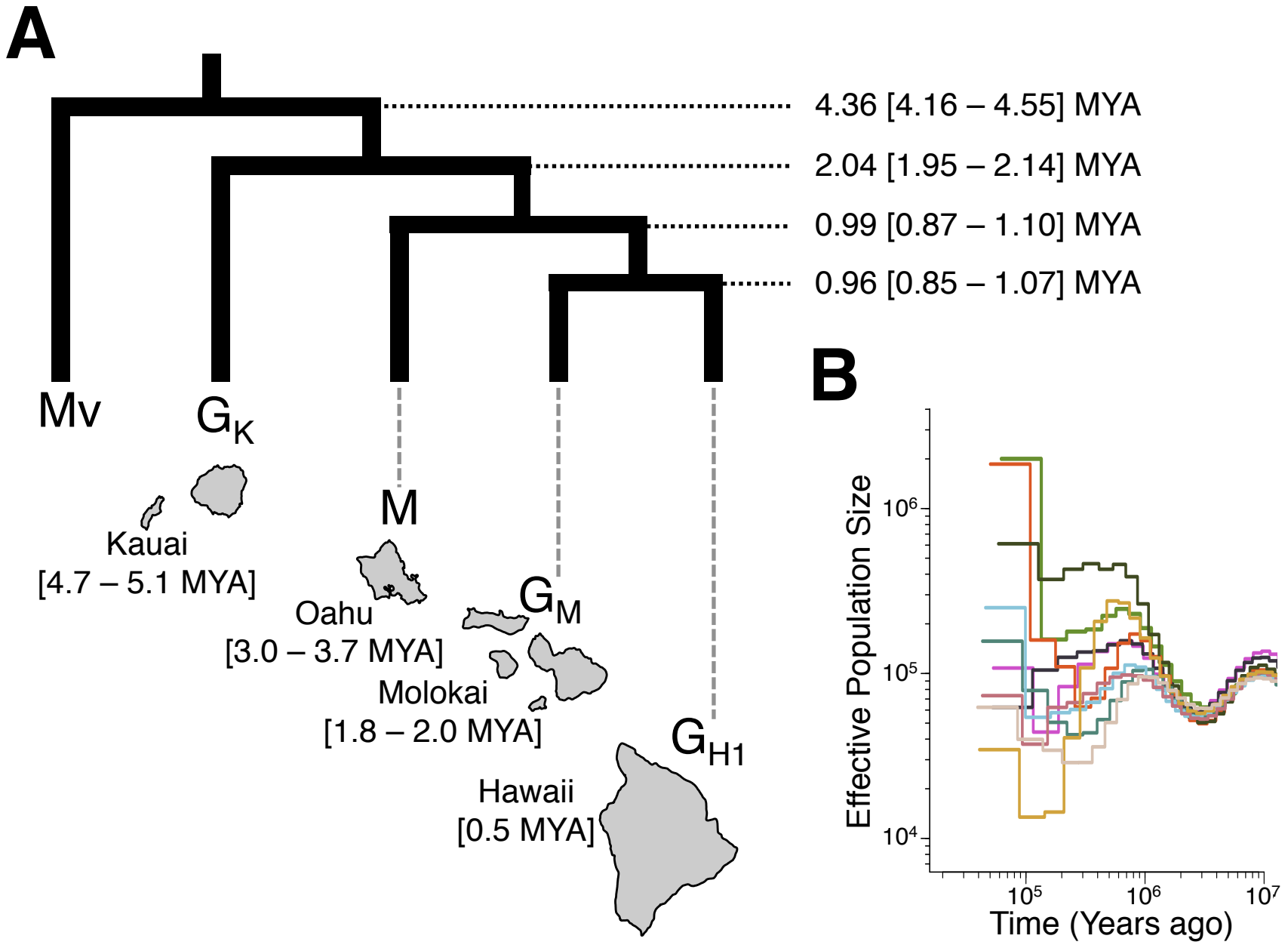
A
4.36 [4.16 – 4.55] MYA
2.04 [1.95 – 2.14] MYA
0.99 [0.87 – 1.10] MYA
0.96 [0.85 – 1.07] MYA
Mv
G_K
Kauai
[4.7 – 5.1 MYA]
M
Oahu
[3.0 – 3.7 MYA]
G_M
Molokai
[1.8 – 2.0 MYA]
G_H1
Hawaii
[0.5 MYA]
B
Effective Population Size
10^6
10^5
10^4
10^5
10^6
10^7
Time (Years ago)

A

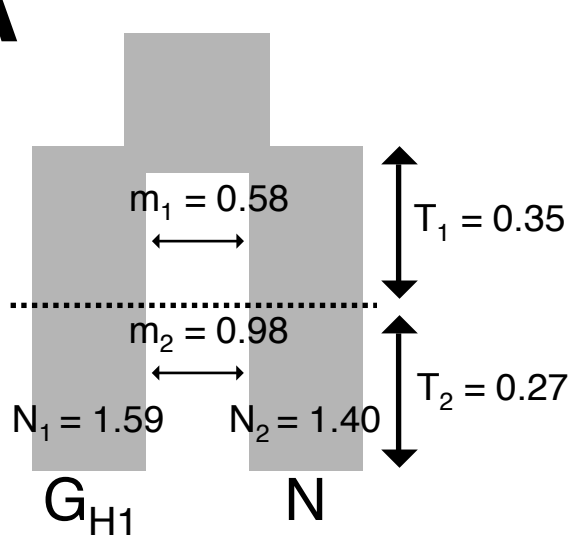
m1 = 0.58
T1 = 0.35
m2 = 0.98
T2 = 0.27
N1 = 1.59
N2 = 1.40
GH1
N

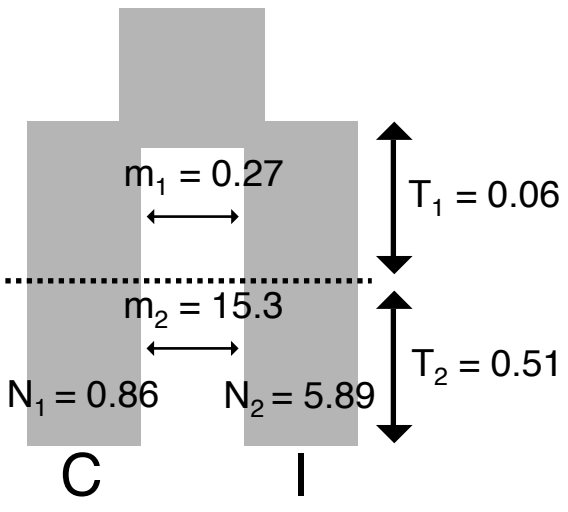
m1 = 0.27
T1 = 0.06
m2 = 15.3
T2 = 0.51
N1 = 0.86
N2 = 5.89
C
I

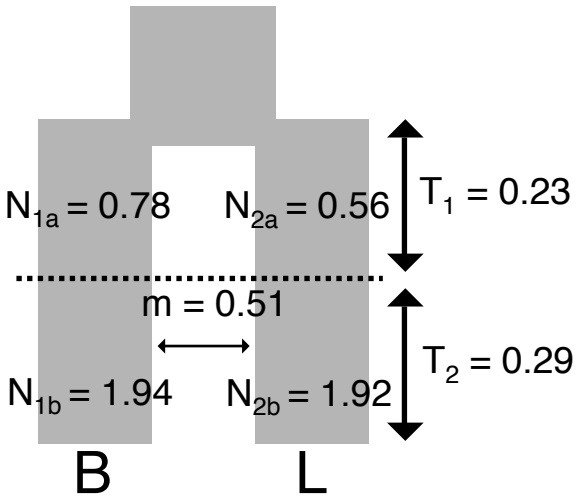
N1a = 0.78
N2a = 0.56
T1 = 0.23
m = 0.51
T2 = 0.29
N1b = 1.94
N2b = 1.92
B
L

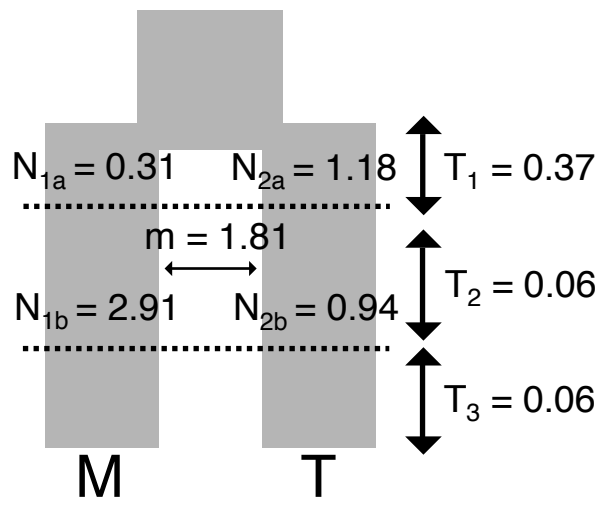
N1a = 0.31
N2a = 1.18
T1 = 0.37
m = 1.81
T2 = 0.06
N1b = 2.91
N2b = 0.94
T3 = 0.06
M
T

B

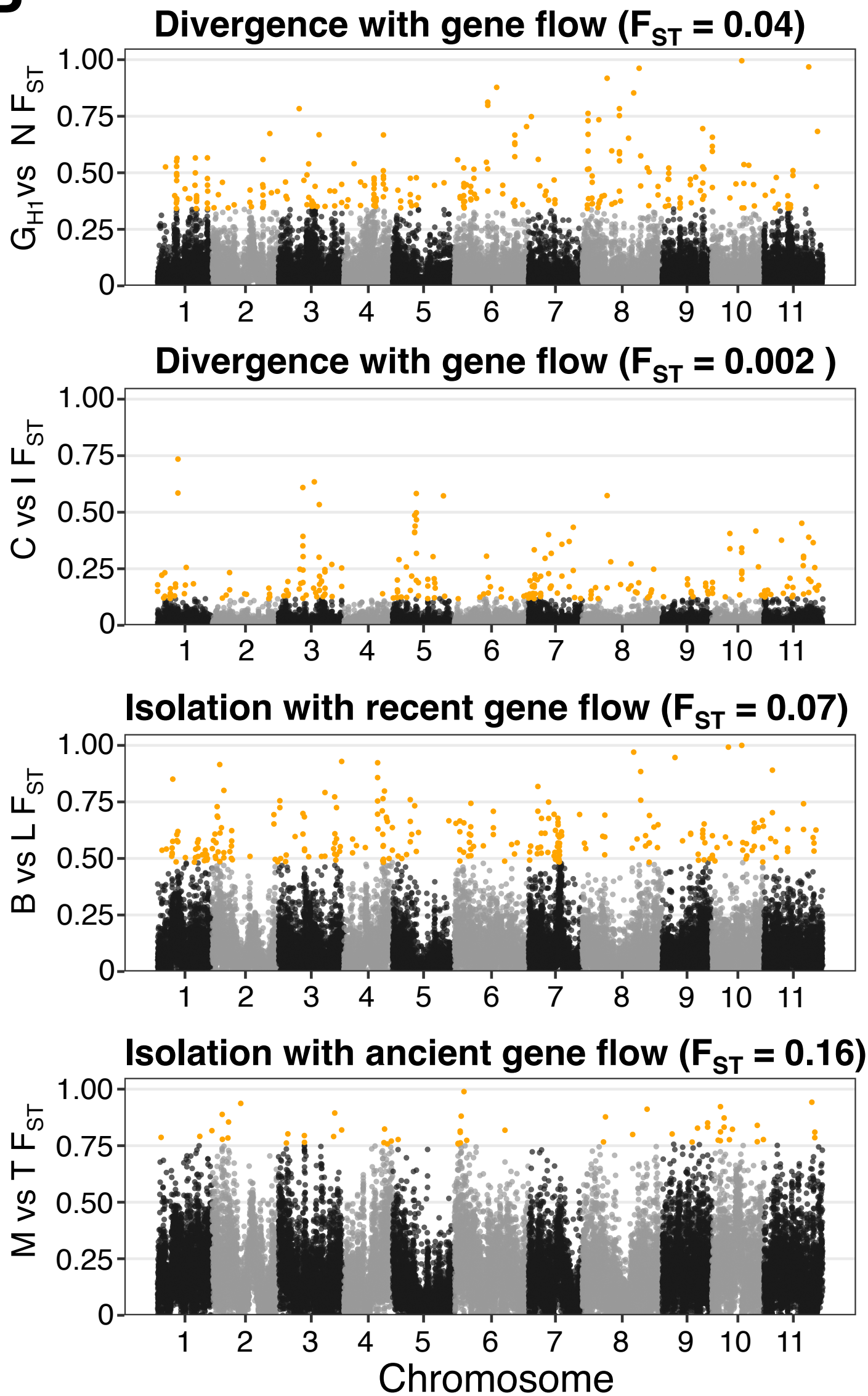
Divergence with gene flow (FST = 0.04)
GH1vs N FST
1.00
0.75
0.50
0.25
0
1 2 3 4 5 6 7 8 9 10 11
Divergence with gene flow (FST = 0.002)
C vs I FST
Isolation with recent gene flow (FST = 0.07)
B vs L FST
Isolation with ancient gene flow (FST = 0.16)
M vs T FST
Chromosome

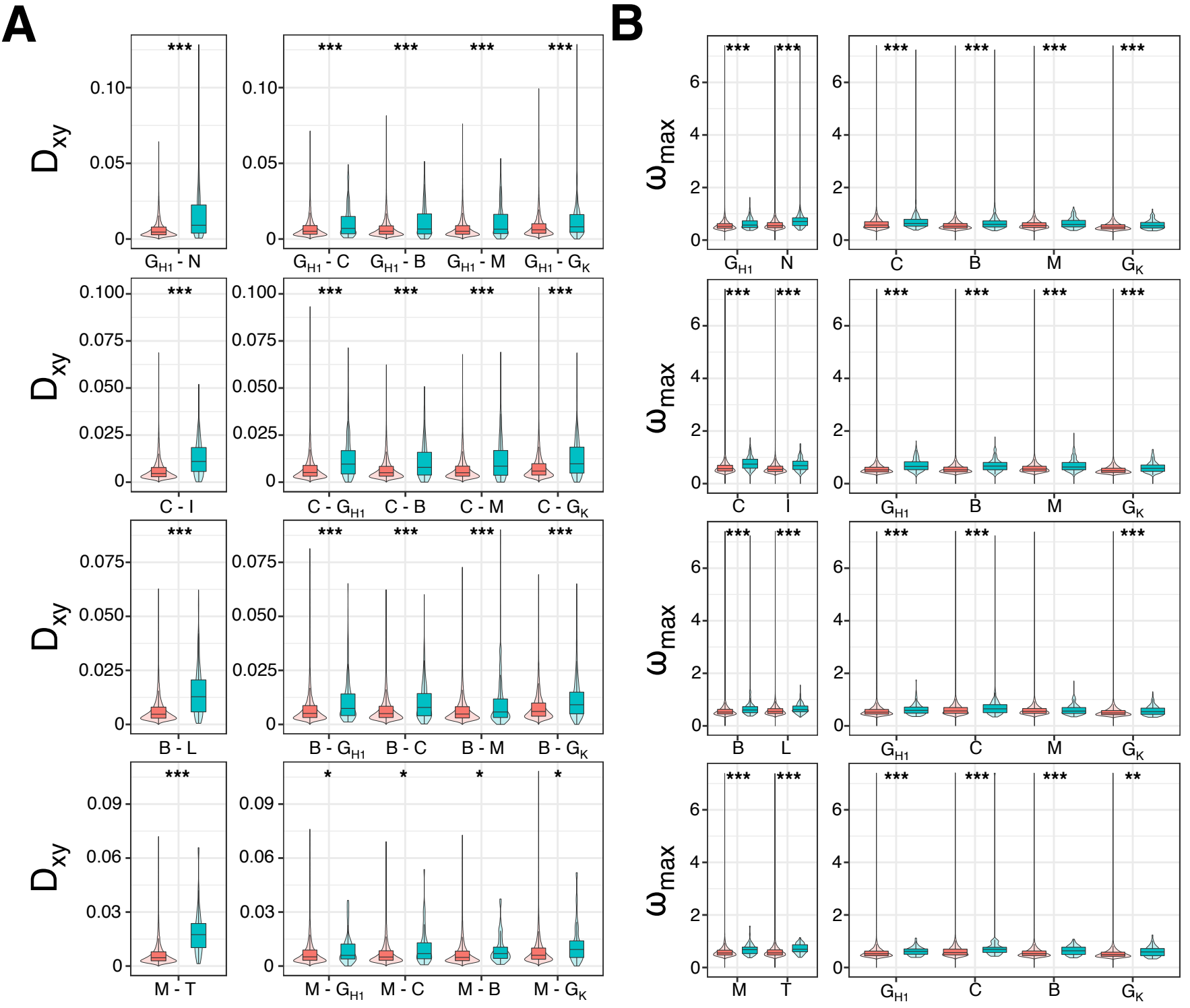
A
B
D_{xy}
ω_{max}
G_{H1} - N
G_{H1} - C
G_{H1} - B
G_{H1} - M
G_{H1} - G_K
C - I
C - G_{H1}
C - B
C - M
C - G_K
B - L
B - G_{H1}
B - C
B - M
B - G_K
M - T
M - G_{H1}
M - C
M - B
M - G_K
G_{H1}
N
C
B
M
G_K
I
L
T
***
**
*